Department of Astronomy – University of Virginia

The Search for Gravitationally Bound Companions to *Kepler* Objects of Interest: an Astrometric Study Using Speckle Imaging Over a Decade

Undergraduate Senior Thesis – ASTR 4998
13 May, 2025

Presented by:
Andrew Heil

Advisors:
Steven Majewski, James Davidson Jr.

This thesis is submitted in partial completion of the requirements of the BA Astronomy Major

Draft version May 13, 2025
Typeset using LaTeX default style in AASTeX631

The Search for Gravitationally Bound Companions to *Kepler* Objects of Interest: an Astrometric Study Using Speckle Imaging Over a Decade

Andrew L. Heil,[1] James W. Davidson Jr.,[1] Steven R. Majewski,[1] and Elliott P. Horch[2]

[1]*Department of Astronomy, University of Virginia*
530 McCormick Road, Charlottesville, VA 22904, USA
[2]*Department of Physics, Southern Connecticut State University*
501 Crescent Street, New Haven, CT 06515, USA

ABSTRACT

We report on the updated dispositions of 37 *Kepler* Objects of Interest with companion stars as either line-of-sight or common proper motion pairs. These targets were previously selected for follow-up from the *Kepler* mission to be observed using speckle imaging to determine whether the stellar pairs were gravitationally bound. Originally flagged as potential exoplanet hosts, these systems were found to have two or more stellar components that could interfere with photometric planetary analysis and potentially impact the study of orbital dynamics of the putative planets if the stellar pairs are gravitationally bound. Previous work on these systems has been updated with relative astrometry and photometry from new speckle observations using DSSI at APO as well as system parameters in *Gaia*'s third data release. The new data have directly improved the dispositions of eight systems and decreased uncertainty across the sample as a whole. We find that 25 of the systems in our sample exhibit common proper motion, five are line-of-sight pairs, and seven remain of uncertain disposition. Additionally, we examined systems within our sample for which Gaia resolved the same components we resolve with speckle imaging. In these nine case, we compare the Bailer-Jones distances for each system component to see if both components are located at the same, or different, distances. When comparing this complimentary technique against our results, we find the two methods largely agree.

Keywords: Speckle interferometry (1552) — Astrometry (80) — Binary stars (154) — Exoplanet System (484)

1. INTRODUCTION

The study of extrasolar planets, or exoplanets for short, is a relatively new and increasingly popular sub-field of astronomy. Exoplanets are planets orbiting stars outside of our own Solar System. Although the first circumstellar, planetary disk was observed by Smith & Terrile (1984), the existence of exoplanets was not confirmed until the 1990's. In 1992, two terrestrial planets were discovered orbiting a pulsar via subtle variations in the millisecond-long radio pulses that were received by Wolszczan & Frail (1992). In 1995, the first exoplanet orbiting a main-sequence star was discovered; a half-Jupiter-mass gas giant planet orbiting at only 0.05 AU was detected via periodic stellar radial velocity variations (Mayor & Queloz 1995). Then, in 1999, both Greg Henry's and David Charbonneau's research teams independently detected a planet transiting the star HD 209458 by observing a periodic drop in the star's flux; this aligned with previous measurements of the star's radial velocity, helping to confirm the transits were of an orbiting body (Henry et al. 2000; Charbonneau et al. 2000). Since then, transit events have become the most successful method of exoplanet detection, accounting for about 75% of all new exoplanet discoveries every year since 2016, greatly surpassing radial velocity, micro-lensing, and other search methods (Deeg & Alonso 2018).

The *Kepler* satellite was launched by NASA in 2009 with the purpose of finding transiting exoplanets orbiting nearby stars in our galaxy. The mission has confirmed the presence of thousands of planets via transit detection and identified thousands more stars as *Kepler* "Objects of Interest" (KOIs) that exhibit transit-like signals in their light curves. Many ground-based follow-up observations have been further applied to these KOIs, such as Youdin (2011), Everett et al. (2015), Hirsch et al. (2017), and Colton et al. (2021). These follow up studies are important to characterize exoplanets accurately as we further understand their range of properties, occurrence rates, and formation histories. The *Kepler* telescope was intentionally designed with a large field of view at the cost of lower spatial resolution, and many of these objects have been found to have companion stars that fall within the same pixel. This source of background flux dilutes transit signals, causing a systematic underestimation of planetary radius (Ciardi et al. 2015). A companion can also be the source of false positive exoplanet detections, especially if it is itself an eclipsing binary (Everett et al. 2015). Therefore, high-resolution ground-based follow-up observations are required to search for and study any companions within the *Kepler* aperture.

A companion star may truthfully be only a line-of-sight (LOS) alignment that forms an optical double with no gravitational binding. However, it may also be a widely separated, gravitationally bound companion, forming a binary system. Observations by Hirsch et al. (2017) looked at many *Kepler* objects with companion stars and utilized photometric analysis to place the star of interest and the companion star on a Hertzsprung-Russell (H-R) diagram—a luminosity vs. color plot—to see if both fell on a shared isochrone. An isochrone (meaning "same time") is a line drawn on an H-R diagram that intersects stars of the same age. Since the two stars of a binary system most often form at the same time as one another, it is unlikely that a companion that lies on a different isochrone from the primary star would be gravitationally bound. The calculations using this method assume both stars to be the same distance, however, and thus can not inherently distinguish between background giants and closer dwarf stars. A complementary approach to isochrone fitting is presented by Colton et al. (2021): The astrometric precision of high-resolution speckle imaging is used to measure the relative positions of double stars over a substantially long period of time. With these data, it is possible to judge the likelihood that the system is either LOS or gravitationally bound based on whether the two stars exhibit common proper motion (CPM). Their study presents data on 57 KOIs, of which 37 had enough speckle observations (3 or more independent observations) for them to analyze and assign dispositions.

The work presented in this thesis aims to improve the dispositions of those 37 targets by continuing the work done in Colton et al. (2021) using new speckle data taken with the Differential Speckle Survey Instrument (DSSI; Horch et al. 2009, Davidson et al. 2024) on the Astrophysical Research Consortium (ARC) 3.5-m telescope at Apache Point Observatory (APO). Our work extends the observational baseline of this program from roughly 8 years to over 13 years for some targets. This allows us to refine the astrometric calculations by better constraining the relative motions of the stellar pairs over a longer time-span. The distances to our targets range from 100-1,000 pc or more, and the typical angular separation is roughly an arcsecond. This corresponds to physical separations of hundreds to thousands of AU, meaning the orbital periods of these companions, if bound, are expected to be hundreds or thousands of years, and thus their positions relative to one another may not change significantly on observable timescales. Therefore, we do not anticipate observing orbital motion except in a small subset of systems (such as those in Davidson et al. 2024 and Section 4.4.3), so we examine the magnitude of change in their relative positions compared to their overall proper motion as evidence of whether the systems are co-moving or just happen to form an optical double along our line of sight.

2. INSTRUMENTS, OBSERVATIONS, AND DATA REDUCTION

To obtain accurate measurements of stars having separations on the order of one arcsecond or less, we make use of speckle interferometry. This allows us to remove the effects of turbulence in the atmosphere, which normally smear the image of a star across the detector far beyond the diffraction limit of the telescope, making many close binaries undetectable without some kind of correction. We take advantage of the fact that these stars are very near one another on the sky, and their light passes through the same or very similar coherence cells before arriving at the telescope (i.e. they are subject to isoplanicity), meaning the paths of light from both stars are affected nearly identically. A speckle image contains many smaller images of the target at the telescope's diffraction limit convolved into a speckle pattern by these atmospheric effects; Figure 1 shows four example speckle patterns for five binary systems of various separations. These images are analyzed using the data reduction techniques discussed in Section 2.3. The end result is a diffraction-limited reconstructed image as well as measurements of the position angle and separation of the two stars.

2.1. *Instruments*

The observational program to which we contribute makes use of speckle observations taken with DSSI, as well as the NN-EXPLORE Exoplanet Stellar Speckle Imager (NESSI; Scott et al. 2018). However, all new observations we present in this study were acquired with DSSI at APO in 2022 and 2023. Designed with the goal of efficiently

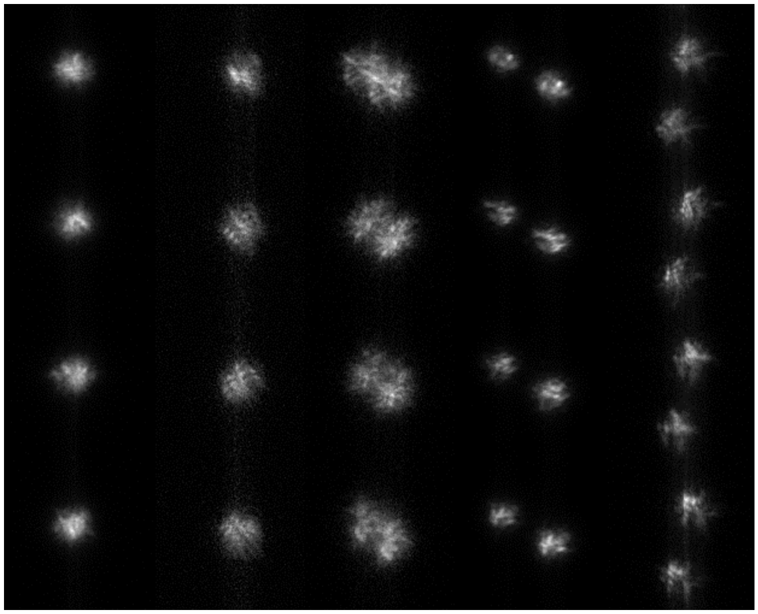

Figure 1. Example speckle patterns of binary systems observed at the WIYN telescope by Hoffmann (2000). Five different systems are shown along the abscissa of this image, varying from small to large separations from left to right. Along the ordinate are four individual frames taken of each system. The doubled speckle patterns are a result of the wavefront from each star passing through the same Fried cells in the atmosphere. At large separations, it is easy to tell the components apart visually, but this becomes more difficult as separation decreases.

obtaining both astrometric and photometric data on small-separation binary stars, DSSI allows us to observe through two filters simultaneously. The early upgrade of CCDs to electron-multiplying CCDs (EMCCDs) on the instrument improved both the efficiency and the effective detection limit due to faster readout times and control of electron gain. As outlined in Davidson et al. (2024), DSSI was first commissioned for use at the WIYN 3.5 m telescope in 2008, after which it was used on the two Gemini 8.1 m telescopes (2012-2018), as well as the Lowell Discovery Telescope (LDT; 2014-2021). It has previously been used to collect data on KOIs with companion stars at all of these locations except Gemini-South, due to the declination of the *Kepler* field, but it had the opportunity to observe the field in its time at Gemini-North (2012-2016). NESSI was commissioned at WIYN in 2016 to image with high angular resolution for the validation and characterization of exoplanets and, serving as a successor, allowed more opportunities for DSSI to be used at the other telescopes. Both Gemini telescopes as well as the LDT have since commissioned their own speckle interferometers, and in early 2022, DSSI was relocated to the ARC 3.5 m telescope at APO.

DSSI collimates light from the telescope, then passes the collimated beam through an optical element known as a dichroic positioned at 45° to the beam. Dichroics transmit certain wavelengths and reflect others. In DSSI, the bluer light is transmitted and the redder light is reflected. Each of these beams passes through its own narrow band filter and is focused onto an EMCCD. The EMCCD that records the transmitted blue light is referred to as "camera A" and the EMCCD that records the red light as "camera B." The image produced by the reflected beam is a mirror image of the transmitted one and is additionally subject to astigmatism. This means that, although our astrometry is relatively simple on images taken with camera A, we must be careful with the measurements from camera B, where the plate scale depends on the position angle of the system. The plate scale can be calibrated by observing either "scale" binary stars or a point source through a slit mask; scale binaries are well-observed systems that have well-known separations in the literature, allowing a faithful comparison between the separation we measure and the established value. With a slit mask, the plate scale can be calculated from measurements of the fringes produced in the speckle pattern from observing a point source; this yields a more precise scale value than using scale binaries since the slit separations and dimensions of the instrument can be measured more precisely than stellar separations. An internal slit mask was installed on DSSI in November of 2022, shortly after arriving at APO. To measure the way plate scale changes with position angle, and to characterize any astigmatism introduced by the dichroic, the slit mask can be rotated for measurements to be taken at many different angles. Figure 2 shows two 0.5 s exposures taken in both channels while rotating the slit mask; the slit mask produces a fringe pattern on the detector, and each spot this produces traces

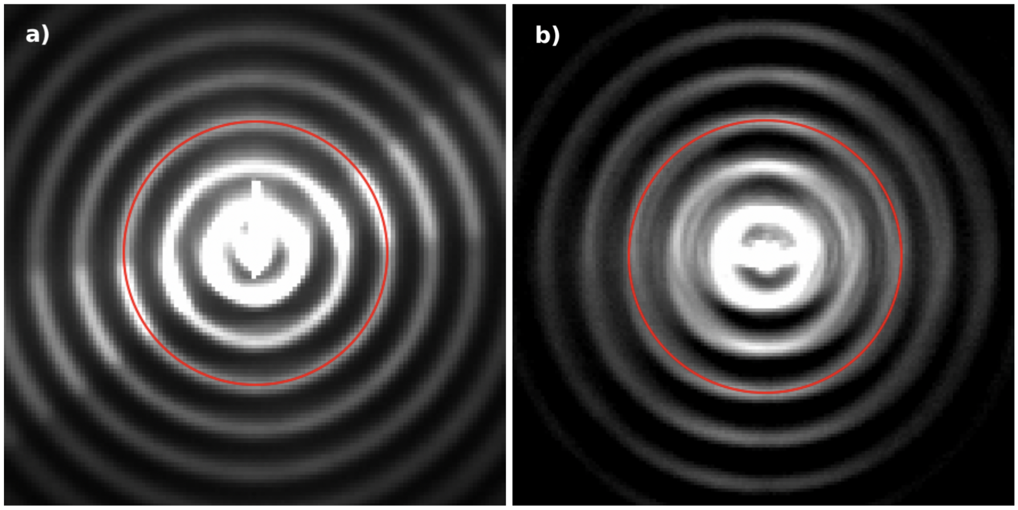

Figure 2. Overlaying a circle on two DSSI slit mask rotation images, we see the circle fits nicely on the image captured through camera A (left, image (a); 692 nm filter), while the circle does not consistently fit the image captured through camera B (right, image (b); 880 nm filter), demonstrating the astigmatism introduced by the dichroic.

out a circle as that pattern rotates with the mask. We digitally overlay a red circle on both images and notice that it fits inside the circular band in camera A's image consistently; however, in camera B, the circle is inconsistent with the circular band, centered at the top and bottom of the image but on the outside edges of the band on the left and right, demonstrating astigmatism in that channel. A good knowledge of plate scale is fundamental to produce precise astrometry as we study the relative motions of small-separation double stars; in the first year of observations with DSSI at APO, the astrometric precision was measured to be 2.06 ± 0.11 mas (Davidson et al. 2024).

2.2. *Observations*

With both DSSI and NESSI, a minimum of 1,000 frames were taken for each observation, and up to 15,000 frames were taken for the faintest targets; the total number of frames taken depended on the target's brightness and observing conditions. Typical integration times per frame were 40 ms at WIYN, LDT, and APO, and 60 ms at Gemini. Longer integration times of ∼100 ms were also used for fainter targets. All DSSI observations used filters centered at wavelengths of 692 nm and 880 nm which have respective FWHMs of 40 nm and 50 nm respectively; observations with NESSI used 562 nm and 832 nm filters with FWHMs of 44 nm and 40 nm respectively. Both instruments used a 256 x 256 pixel sub-array to read out images from each detector.

Observations taken with DSSI and NESSI are broken into 'blocks' that consist of a target star or binary, in our case a KOI, and a point source that is nearby on the sky. A typical 1,000 frame sequence takes less than 2 minutes to complete, and the full block (binary and point source) can be as short as five minutes including overhead time for moving the telescope and centering the images on the detectors; this allows a large list of observations to be tackled efficiently by two observers. Typically, one observer manages the target list, slews the telescope betweem targets, plans the order of observations to maximize efficiency, and updates the observing log. The other observer manages the observations. This includes monitoring the focus of the telescope, adjusting the telescope's position to center the target in both camera frames, adjusting the gain of both EMCCDs and, for particularly faint targets, adjusting the exposure time to ensure ample counts (peaking around 1,000) are recorded. After starting a series of exposures, the star's position is monitored to ensure the speckle patterns do not drift too near one edge of the sub-array.

The previous work in Colton et al. (2021) analyzed the relative proper motions of *Kepler* double stars between 2010 and 2017, a long enough time to begin the determination of systems being either LOS or CPM pairs given the high astrometric precision of speckle imaging. New data have now been collected with DSSI at APO over five different observing runs—2022 September 27 to 30, 2022 November 12 to 16, 2023 May 9 to 12, 2023 September 1 to 2, and 2023 October 19 to 20—extending the total observation baseline to over 13 years for certain systems. Some of the new DSSI data from APO has previously been reported by Davidson et al. (2024), but the majority of it is presented here for the first time. In making effective use of observing time during these runs, our data were taken in parallel with

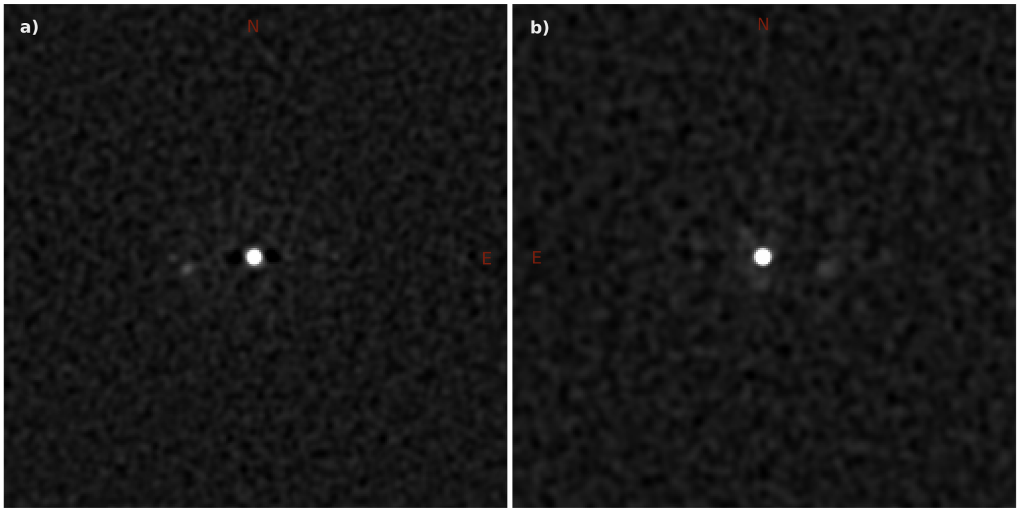

Figure 3. Reconstructed images of KOI-2754 taken with DSSI at APO. Image (a) on the left is from camera A (692 nm), and image (b) on the right is from camera B (880 nm). The companion star ($\Delta m \approx 3$) can be seen to the west and slightly south of the primary—note that camera B is mirrored from camera A. The distortion of the central peak is due to saturation and blooming.

other speckle observation programs, e.g., Steven Majewski's work on quadruple-eclipsing binary systems and Todd Henry's study of K dwarf stars.

2.3. *Data Reduction*

The data reduction methodology has remained the same as described in Horch et al. (2009, 2011, and most recently 2021), but is summarized here in brief. The observations are stored as FITS data cubes in 1,000-frame blocks. Each individual frame is Fourier transformed to provide a power spectrum, and the final power spectrum for the observation as a whole is obtained by summing the individual power spectra of all frames in its block. Another power spectrum is computed for a point source that was observed either shortly before or shortly after the science target. The power spectrum of the science target is then divided by that of the point source in Fourier space to remove the effects of the atmosphere. This deconvolution of the science target and the atmosphere gives the pure power spectrum of the source from which the separation, position angle, and magnitude difference of the components can be accurately measured. To create a reconstructed image of the stars, we must take the inverse Fourier transform of the target. This is calculated by first finding the phase; speckle frames are used to compute subplanes of the image bispectrum (i.e., the Fourier transform of the triple correlation function of the image), which are then summed and used to find the phase via the relaxation technique described in Meng et al. (1990). The phase is then combined with the square root of the source power spectrum to compute the Fourier transform of the target. This is low-pass-filtered to reduce noise and finally inverse-transformed to produce a reconstructed image, as in Figure 3. These images are used to identify the presence of a companion star, but may also be used to cross-check ρ and θ measurements, as we do with KOI-2754 (see Section 4.4.4).

When examining the autocorrelation function of a double star, the secondary component produces a symmetric peak on either side of the primary. This means that that secondary may be assumed to be on the wrong side—most commonly a result of poor data or a small magnitude difference between components—and leads to a measurement of the position angle which is off by 180°, as noted in Table 5 (all speckle measurements). These "flips" can be identified and manually changed if the position angles appear inconsistent between measurements, on the order of 180°; however, some systems, such as KOI-4399 which we do not analyze, lack an ample number of observations to determine which quadrant the secondary is truly in, so there remains a 180° ambiguity in the reported position angle measurements.

3. ANALYSIS

3.1. *Analyzing Proper Motions*

Table 1. Proper motions and parallaxes of 37 KOIs

KOI no.	Speckle $\Delta\mu_\alpha$ mas·yr^{-1}	Speckle $\Delta\mu_\delta$ mas·yr^{-1}	System μ_α mas·yr^{-1}	System μ_δ mas·yr^{-1}	π mas	Source for μ and π^a
1	0.920 ± 0.462	-1.200 ± 0.671	5.434 ± 0.015	1.572 ± 0.016	4.631 ± 0.012	DR3
13	0.129 ± 0.357	0.067 ± 0.335	-4.411 ± 0.042	-15.220 ± 0.050	2.032 ± 0.034	DR3^b
98	-0.499 ± 0.207	0.348 ± 0.152	-0.1 ± 1.1	-10.6 ± 1.0	1.449 ± 0.113	UCAC4, CFOP
118	-16.526 ± 0.932	-42.944 ± 0.645	14.366 ± 0.010	35.518 ± 0.010	2.115 ± 0.009	DR3^b
120	1.153 ± 0.865	-1.186 ± 0.592	-7.067 ± 0.029	-12.232 ± 0.029	1.227 ± 0.023	DR3^b
177	0.716 ± 0.118	0.238 ± 0.161	5.5 ± 3.5	6.1 ± 1.4	2.160 ± 0.335	UCAC4, CFOP
258AB	1.453 ± 0.465	0.935 ± 0.277	4.143 ± 0.018	-7.632 ± 0.020	2.576 ± 0.016	DR3
258AC	-8.969 ± 1.157	-3.406 ± 0.976	4.143 ± 0.018	-7.632 ± 0.020	2.576 ± 0.016	DR3
270	2.329 ± 0.074	0.694 ± 0.137	-9.4 ± 1.9	-44.4 ± 1.7	3.845 ± 0.194	Tycho-2, CFOP
279	-0.296 ± 0.306	0.712 ± 0.481	4.210 ± 0.018	6.644 ± 0.021	2.076 ± 0.015	DR3
284	-0.360 ± 0.227	-0.316 ± 0.188	-21.100 ± 0.055	-0.781 ± 0.061	2.628 ± 0.048	DR3^b
307	2.464 ± 0.918	0.655 ± 0.587	-4.117 ± 0.120	-3.998 ± 0.122	1.270 ± 0.109	DR3
640	1.519 ± 0.765	-1.717 ± 0.970	-27.1 ± 2.4	-18.2 ± 2.3	2.823 ± 0.325	UCAC4, CFOP
959	-0.835 ± 0.348	-2.796 ± 0.492	-151.584 ± 0.452	-397.878 ± 0.453	28.041 ± 0.462	DR3^b
976	0.309 ± 0.295	1.756 ± 0.111	-1.6 ± 1.2	4.0 ± 1.1	3.625 ± 1.155	Tycho-2, CFOP
977	0.311 ± 0.294	0.259 ± 0.346	-3.836 ± 0.072	-1.838 ± 0.072	0.857 ± 0.057	DR3
980	0.567 ± 0.316	0.257 ± 0.311	1.622 ± 0.021	-6.880 ± 0.020	1.132 ± 0.016	DR3^b
984	0.577 ± 0.227	0.017 ± 0.607	1.589 ± 0.014	7.852 ± 0.015	4.324 ± 0.013	DR3^b
1119	1.768 ± 0.682	-3.986 ± 0.863	26.917 ± 0.030	17.662 ± 0.030	8.504 ± 0.025	DR3
1150	-2.033 ± 0.922	0.006 ± 0.472	-9.546 ± 0.234	-11.124 ± 0.271	0.433 ± 0.217	DR3
1531	-0.184 ± 0.834	-0.585 ± 1.297	6.111 ± 0.278	12.443 ± 0.237	3.117 ± 0.182	DR3
1613	-0.066 ± 0.283	1.351 ± 0.332	-18.780 ± 0.538	-20.457 ± 0.581	2.031 ± 0.501	DR3
1792AB	-20.120 ± 0.715	-28.178 ± 2.210	13.980 ± 0.123	26.197 ± 0.138	1.403 ± 0.115	DR3
1792AC	-22.982 ± 1.366	-30.048 ± 1.944	13.980 ± 0.123	26.197 ± 0.138	1.403 ± 0.115	DR3^b
1890	-0.163 ± 0.474	1.213 ± 0.259	-0.734 ± 0.127	-14.569 ± 0.134	2.030 ± 0.118	DR3
1962	0.561 ± 0.285	-0.899 ± 0.075	10.478 ± 0.607	-7.023 ± 0.582	0.908 ± 0.330	DR2
2059	-1.496 ± 0.653	-1.189 ± 0.406	5.531 ± 0.542	7.938 ± 0.624	2.662 ± 0.445	DR3
2754	0.945 ± 0.181	-0.067 ± 0.277	-14.093 ± 0.023	11.108 ± 0.028	2.873 ± 0.022	DR3
2837	2.408 ± 0.940	1.421 ± 0.929	0.572 ± 0.183	-3.159 ± 0.183	0.975 ± 0.096	DR3
2904	-1.777 ± 1.267	1.509 ± 0.787	5.584 ± 0.034	2.855 ± 0.037	1.189 ± 0.031	DR3
3020	1.208 ± 1.469	0.532 ± 2.955	1.162 ± 0.135	-2.316 ± 0.153	0.588 ± 0.119	DR3
3156	1.270 ± 0.366	2.812 ± 0.339	-6.933 ± 0.080	-5.713 ± 0.087	8.322 ± 0.075	DR3^b
3214AB	-0.468 ± 0.347	0.338 ± 0.589	2.930 ± 0.381	7.917 ± 0.416	2.122 ± 0.357	DR3
3214AC	1.119 ± 1.569	-1.057 ± 1.029	2.930 ± 0.381	7.917 ± 0.416	2.122 ± 0.357	DR3^b
4287	0.911 ± 0.201	-0.627 ± 0.102	-15.918 ± 0.075	-26.065 ± 0.088	2.426 ± 0.063	DR3
5578	2.125 ± 0.108	-0.183 ± 0.121	-2.608 ± 0.483	15.478 ± 0.457	3.354 ± 0.379	DR3
5822	-0.265 ± 0.216	0.979 ± 0.550	18.8 ± 2.2	15.0 ± 6.5	6.852 ± 0.741	UCAC4, CFOP

[a] Source abbreviations are: DR2 = Gaia Collaboration et al. (2018), DR3 = Gaia Collaboration et al. (2023), UCAC4 = Zacharias et al. (2013), Tycho-2 = Høg et al. (2000), CFOP = *Kepler* Community Follow-up Observing Program https://exofop.ipac.caltech.edu/tess.

[b] System is resolved by *Gaia*, so the listed system μ and parallax belong to the primary star.

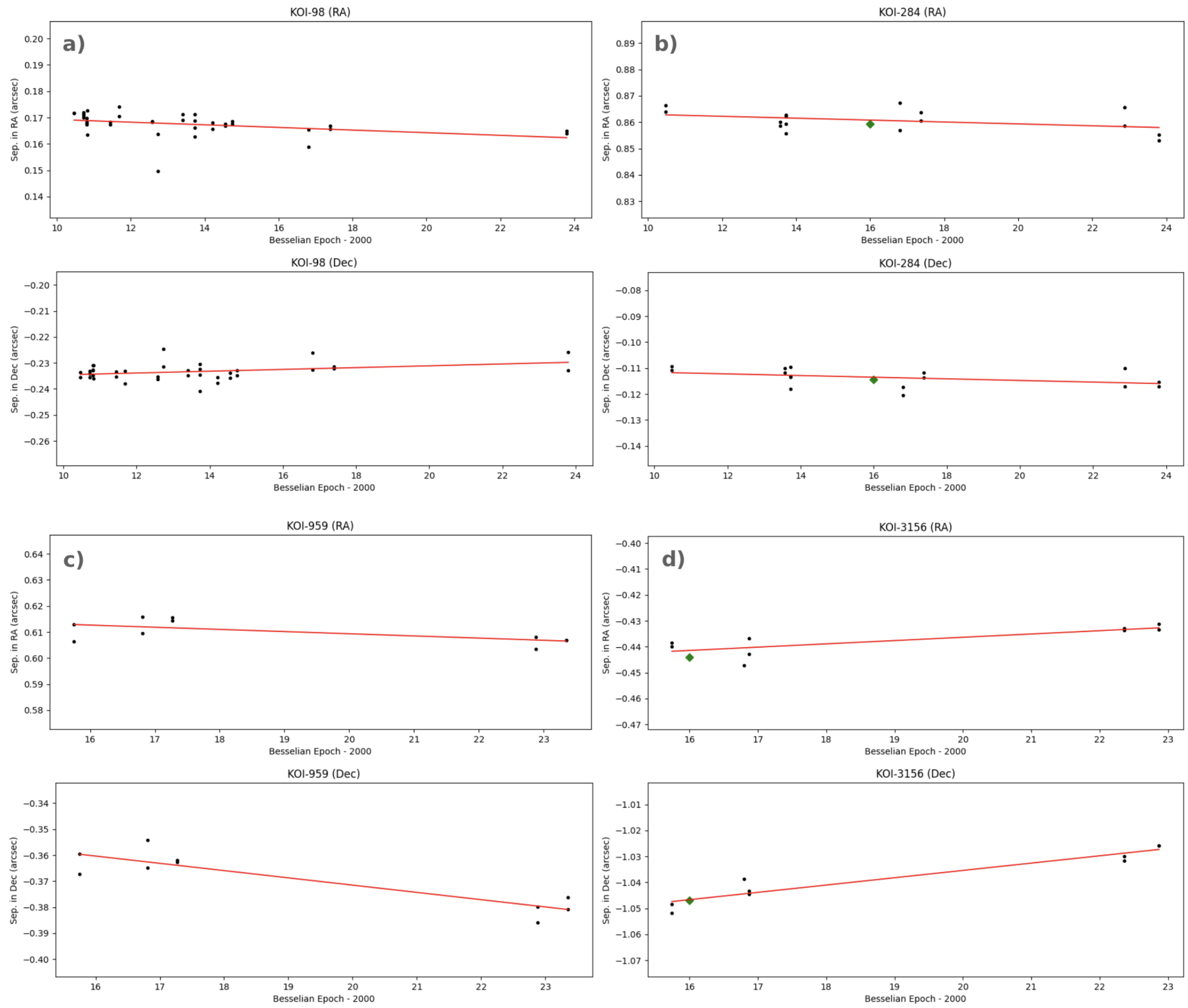

Figure 4. Separations in RA and declination of four KOI double star systems. KOI-284 and KOI-3156 are resolved by *Gaia*, so we include a data point from *Gaia* DR3 on their plots labeled with a green diamond—these points are only for reference and are not included in the calculations of best fit lines. a) KOI-98 is an example of a CPM pair with extensive observations; b) KOI-284 is another CPM pair where we see *Gaia*'s positions are in agreement with our measurements; c) KOI-959 was previously of uncertain disposition, but is now thought to be a CPM pair with the addition of the two most recent observations; d) KOI-3156 is of uncertain disposition, but the distances to its components suggest it is likely to be a CPM pair (see Table 4 and Section 4.3 for further discussion).

We use the results from our speckle observations to study the change in a companion's position over time. We calculate the relative proper motion $\Delta\mu$ of the secondary star with respect to the primary by plotting their separation as a function of time, which we do in both right ascension and declination components separately (as in Figure 4). The slope of the best fit line for each component of the relative proper motion is derived in arcseconds per year, and the two vector components can be summed to find the average relative proper motion vector. We report results in Table 1, which lists the KOI number in column 1, relative proper motion from speckle in both RA and Dec in columns 2 and 3, respectively, the system proper motion from *Gaia* in both RA and Dec in columns 4 and 5, the *Gaia* parallax in column 6, and the source for the system proper motion and parallax in column 7. In cases where *Gaia* DR3 lists results for both the of the resolved speckle components, we list values associated with the brighter of the two stars. We examine this in more detail in Section 4.3.

As first presented in Colton et al. (2021), there are two measurements that can be made to determine if a system is CPM or LOS. The first is the ratio of the relative proper motion to the system proper motion μ_1, referred to as R_1:

$$R_1 = \frac{|\Delta\mu|}{|\mu_1|} \tag{1}$$

By taking a ratio, we can account for the fact that average proper motions decrease with distance. For a co-moving system, the ratio R_1 should be near zero: We expect μ_1 to be much greater than our measured $\Delta\mu$. If the secondary star is a dim foreground contaminant, then its proper motion should dominate $\Delta\mu$ and be greater than that of the primary, making the ratio exceed one. Conversely, if the secondary is a background companion, then the primary's proper motion should dominate $\Delta\mu$, making it roughly the same as μ_1 and the ratio roughly equal to one. Colton et al. (2021) select two random samples of stars in the *Kepler* field from *Gaia* DR2 and form 1,366 hypothetical optical doubles between them. They calculate $|\Delta\mu|/|\mu_1|$ for each of the hypothetical doubles and find that the median value lies around one, as expected. The exercise also shows that <5% of optical doubles have R_1 ratios less than 0.32; we later use this value as an upper limit on R_1 for systems to be considered a CPM pair. The median line and 5% cutoff are shown later in Figure 5 in relation to the R_1 values of our 37 KOIs.

The second way to analyze the motions is through the ratio of the relative proper motion to the expected relative proper motion if the system were gravitationally bound and undergoing orbital motion, referred to as R_2:

$$R_2 = \frac{|\Delta\mu|}{|\Delta\mu_{avg,orb}|} \tag{2}$$

For a bound system (and a proper estimation of $\Delta\mu_{avg,orb}$), the orbital motion should be roughly equal to the relative proper motion we observe, meaning the R_2 ratio should be near one. This is because the two stars will be co-moving through the sky and will only change position relative to one another as they trace out orbital paths. If the R_2 ratio greatly exceeds one, then the average relative motion is much greater than what is possible for a gravitationally bound system and the pair is likely to be LOS.

The estimation of $\Delta\mu_{avg,orb}$ based on observational data is described in Colton et al. (2021), but outlined here. The orbital period of the system can be found with Kepler's harmonic law, using the observed average separation ρ, system parallax π, and estimated total mass of the system M_{tot}. The separation is averaged across all filters and epochs for each system. The total mass is obtained by first estimating the mass and absolute V magnitude of the primary star from its temperature, then estimating the secondary's absolute V magnitude—and subsequently its mass—based on the magnitude difference in the 692 nm (or 562 nm) filter. All stars were assumed to be on the main sequence except for two, KOI-258 and KOI-977, which SIMBAD lists as giants. The secondary's mass estimate relies on an assumption that the two components are at the same distance, and it is thus unreliable if the system is found to be LOS and unbound.

The perimeter of the observed orbital ellipse is then calculated. It depends on many different properties of the system's geometry—eccentricity, inclination, and ascending node—but the average perimeter is simply equal to some geometrical factor times the semimajor axis of the orbit, which we take to be the system's average separation. Colton et al. (2021) construct a sample of 5,000 binary systems with random orientations and distribute their distances across a Gaussian that matches the mean and standard deviation of their observed sample. Across all of the systems, they find the average geometrical factor to be roughly 4.6. Finally, the average orbital velocity is found by dividing the perimeter of the orbital ellipse by the orbital period, giving a distance traveled per year. Thus we calculate $\Delta\mu_{avg,orb}$ and R_2 as follows:

$$|\Delta\mu_{avg,orb}| = \frac{4.6 \cdot \rho}{P} = 4.6 \cdot \rho \cdot \sqrt{\frac{\pi^3 M_{tot}}{\rho^3}} \tag{3}$$

$$R_2 = \frac{|\Delta\mu|}{4.6}\sqrt{\frac{\rho}{\pi^3 M_{tot}}} \tag{4}$$

Using the same simulation, they calculate a $|\Delta\mu|$ value at a random point in each orbit. R_2 values for the simulated systems cluster around one regardless of distance, and only 5% of binaries have an $R_2 > 1.87$; this is used as an upper limit for systems to be considered CPM since values greater than this indicate relative motion inconsistent with orbital motion. The median value from their simulation as well as the 95% cutoff are shown on the $\log(R_2)$ versus distance plot in Figure 5.

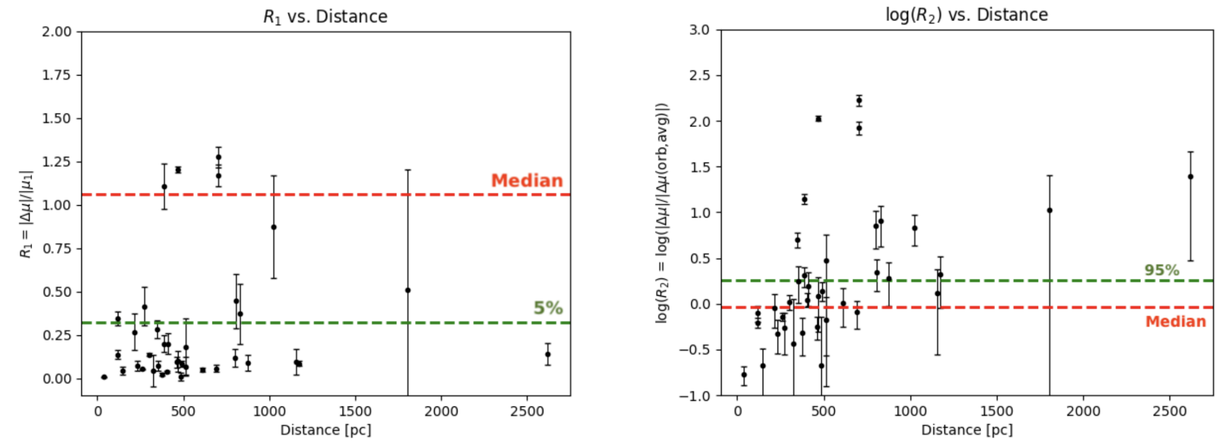

Figure 5. Plots of R_1 (left) and $\log(R_2)$ (right) values against distance for 37 KOIs (Table 2). As discussed in Section 3.1, the red dashed line in the left plot marks the median R_1 value calculated for a set of simulated optical doubles; the green 5% line marks the upper limit on R_1 for systems to be judged as CPM. The red dashed line in the right plot marks the median $\log(R_2)$ value for a set of simulated binary systems; here, the green 95% line marks the upper limit on a $\log(R_2)$ value for the system to be CPM.

3.2. *Assigning Dispositions*

The values of each system's R_1 and R_2 ratios provide information about the likelihood of it being a LOS double or a CPM pair, which we use to define its disposition as either. Following the analysis of the previous section, we conclude that systems with an R_1 value greater than 0.32 are more likely to be LOS than co-moving, and an R_2 value greater than 1.87 indicates relative motion that is not consistent with orbital motion. With these limits, we follow the same requirements for reporting the dispositions of targets as Colton et al. (2021). These are as follows, where δR_1 and δR_2 are the respective uncertainties:

1. "CPM" systems must have $R_1 + \delta R_1 < 0.32$ and $R_2 - \delta R_2 < 1.87$. These systems have their full range of R_1 values including uncertainties below the 5% line and a range of R_2 values that overlap with the range of potential orbital motion.

2. "CPM?" systems have $R_1 < 0.32$ and $R_2 - \delta R_2 < 1.87$. These systems have measured R_1 values below the 5% line but an R_1 uncertainty interval that includes values greater than 0.32. The same restriction on R_2 as for "CPM" systems requires consistency with orbital motion.

3. "LOS" systems have $R_1 - \delta R_1 > 0.32$ and $R_2 - \delta R_2 > 1.87$. The full range of R_1 values is above the 5% cutoff, and the full range of R_2 values is above the 95% cutoff; we are confident that the motions of the two stars in these systems are independent and do not correspond to orbital motion.

4. Any systems that do not fall into one of these three categories are considered "Uncertain".

3.3. *Updating the Data*

To provide an accurate update to the results given in Colton et al. (2021), we followed the methodology described in their paper by building Python code that could both reproduce their results and incorporate new data. The notebook takes in observational data in the format of Table 5 (Appendix A) and calculates $\Delta\mu_\alpha$, $\Delta\mu_\delta$, R_1, and R_2 values, assigns a disposition of CPM, CPM?, LOS, or Uncertain to each target, and produces plots such as Figures 4 through 8. The process for writing the notebook is briefly outlined here, and screenshots are attached in Appendix B.

The first—and perhaps most important—functionality of the code is the ability to replicate the previously reported results when given the same initial data. This builds confidence that the process, math, and general logic throughout the code are correct. To accomplish this, the code reads in the observational data provided in Table 1 of Colton et al. (2021), as well as the parallax and system proper motion values from their Table 2; it stores the relevant data from these tables (primarily observation date, position angle θ, separation ρ, parallax π, μ_α, and μ_δ) in dictionaries linking KOI number with the corresponding list of measurements so the data are organized and easily accessible. The $\Delta\mu_\alpha$

and $\Delta\mu_\delta$ for each system are calculated by plotting the right ascension and declination components of separation over time (as in Figure 4) and performing a least squared linear fit. After summing $\Delta\mu_\alpha$ and $\Delta\mu_\delta$ to get $|\Delta\mu|$, and μ_α and μ_δ to get $|\mu_1|$, R_1 values are calculated using Equation 1. To produce R_2, average separations are calculated from the lists of separation measurements previously stored in a dictionary, and masses are obtained from Table 3 of Colton et al. (2021); these are combined with $|\Delta\mu|$ using Equation 4. With R_1, R_2 and their respective uncertainties in hand, we are finally able to implement the criteria for assigning dispositions—as outlined in the previous section—and ensure the final results are consistent.

The updated data for ρ, θ, π, μ_α and μ_δ[1] were incorporated once we confirmed the general machinery of the code works properly. Data from *Gaia* were manually pulled from the *Gaia* archive, and APO data were read into the code from a reduced file of measurements. The new values were appended to the corresponding lists of measurements for each system, allowing us to produce the $\Delta\mu_\alpha$ and $\Delta\mu_\delta$ values reported in Table 1 as well as the R_1 and R_2 values and final dispositions in Table 2. A complete list of all speckle measurements, including those in Colton et al. (2021), APO observations previously reported in Davidson et al. (2024), and new APO observations reported here for the first time, are included in Appendix A Table 5.

4. RESULTS

4.1. *Updated Dispositions*

We present updated dispositions for the 37 systems reported in Colton et al. (2021), 27 of which have been observed at APO. The new data in *Gaia* DR3 provide a reason to update all of the systems, even if there were no new speckle observations. Of these 37 systems, we report that 23 are CPM, two are CPM?, five are LOS, and seven are Uncertain. For each system, both the updated disposition as well as the previous disposition are given in columns 8 and 9 of Table 2, respectively. This table also includes: The *Kepler* system number or planetary disposition if unavailable (column 2), the distance to the primary component (column 3), the mass of both components (columns 4 and 5), and the R_1 and R_2 values (columns 6 and 7). Systems with a *Kepler* number are confirmed to have at least one exoplanet. The other planetary dispositions are: Confirmed planets (CP) that have not been given a *Kepler* number, planetary candidates (PC), and false positives (FP). Planetary dispositions for systems without a *Kepler* number are drawn from the *Kepler* Community Follow-up Observing Program.[2] If a parallax is available in the *Gaia* catalog, we report the distance from Bailer-Jones (DR3 2023 or DR2 2018 if unavailable); this distance takes into account the distribution of stellar velocities in the galaxy and uses both parallax and proper motion information to provide a more accurate estimation than simply an inverted parallax for stars in the *Gaia* catalog.

A change in disposition could be the result of one or more updated variables. The introduction of data from *Gaia* DR3 affects $|\mu_1|$ in R_1 (Eq. 1) and π in R_2 (Eq. 4); new speckle data affect $|\Delta\mu|$ in both R_1 and R_2 as well as the average separation ρ in R_2. The uncertainties in each variable of course contribute to δR_1 and δR_2 as well. In general, DR3 reports lower uncertainties than DR2 or other sources, and we find that increasing the number of speckle measurements tends to reduce the uncertainty in relative proper motion and average separation.

Eight systems have changed disposition since Colton et al. (2021); seven of these are now CPM and were previously either CPM? or Uncertain, and one system changed from Uncertain to LOS. All of these systems are considered to have "improved" disposition since they were previously in a statistical gray area and now fall firmly within the categories of either CPM or LOS. The effect of *Gaia* DR3 data can be seen in two of the systems we analyze that were not observed at APO; KOI-2059 was CPM? and is now CPM; KOI-2837 was Uncertain and is now LOS. Neither system had a proper motion or parallax in DR2, and the values for μ_α and μ_δ provided in DR3 have changed significantly from those reported in UCAC4 (Zacharias et al. 2013). KOI-2059 was previously CPM? due to a relatively high δR_1 that pushed the uncertainty interval above the threshold; this was driven by high uncertainties in μ_α and μ_δ from UCAC4. Those uncertainties reported in *Gaia* DR3 are roughly a factor of 5 lower, bringing the $R_1 \pm \delta R_1$ interval below the threshold for CPM. KOI-2837 was previously Uncertain due to a high R_2 value—inconsistent with orbital motion—despite having an R_1 value that indicated the system may be co-moving. The system proper motion is now reported as much slower in DR3, leading to an increase in R_1 and indicating the two components are not exhibiting

[1] We do not update the total mass (M_{tot}) estimates in our analysis because we believe the stellar temperature measurements have not changed significantly. Additionally, it is shown in Colton et al. (2021) that the statistical results of R_2 calculations on the simulated binaries are not strongly dependent on mass estimates.

[2] https://exofop.ipac.caltech.edu/tess/

Table 2. Final values and dispositions

KOI no.	Kepler no. or planetary disp.	Distance pc	M_1 $M_\odot$	M_2^b $M_\odot$	R_1	R_2	Updated disposition	Previous disposition[c]
1[a]	Kepler-1	$213.9^{+0.5}_{-0.6}$	0.97	0.51	0.267 ± 0.106	0.90 ± 0.36	CPM?	CPM?
13[a]	Kepler-13	$488.0^{+9.6}_{-8.4}$	1.6	1.48	0.009 ± 0.022	0.21 ± 0.51	CPM	CPM
98[a]	Kepler-14	690.1 ± 55.7	1.4	1.12	0.057 ± 0.019	0.81 ± 0.27	CPM	CPM
118	Kepler-467	$469.3^{+2.4}_{2.0}$	0.89	(0.46)	1.201 ± 0.018	106.22 ± 7.03	LOS	LOS
120[a]	FP	$802.6^{+15.1}_{-12.3}$	1.12	(1.00)	0.117 ± 0.052	7.19 ± 3.22	Uncertain	Uncertain
177	CP	463.0 ± 71.8	1.00	0.92	0.092 ± 0.032	0.56 ± 0.16	CPM	CPM
258AB[a]	FP	$386.4^{+2.7}_{-2.2}$	1.33	0.72	0.199 ± 0.048	2.03 ± 0.50	CPM	CPM
258AC[a]	FP	$386.4^{+2.7}_{-2.2}$	1.33	(0.52)	1.105 ± 0.131	14.04 ± 1.76	LOS	LOS
270[a]	Kepler-449	260.1 ± 13.1	0.84	0.77	0.054 ± 0.003	0.72 ± 0.07	CPM	CPM
279[a]	Kepler-450	$470.8^{+3.7}_{-3.5}$	1.26	0.67	0.098 ± 0.058	1.22 ± 0.73	CPM	CPM
284[a]	Kepler-132	$378.5^{+8.0}_{-6.7}$	1.19	1.02	0.023 ± 0.010	0.48 ± 0.21	CPM	CPM
307	Kepler-520	$806.0^{+136.4}_{-80.2}$	1.12	(1.10)	0.444 ± 0.157	2.21 ± 0.84	Uncertain	Uncertain
640	Kepler-632	354.2 ± 40.8	0.79	0.70	0.070 ± 0.028	1.78 ± 0.76	CPM	CPM
959[a]	FP	35.4 ± 0.6	0.24	0.22	0.007 ± 0.001	0.17 ± 0.04	CPM	Uncertain
976[a]	FP	275.9 ± 87.9	1.50	(1.19)	0.414 ± 0.111	0.54 ± 0.26	Uncertain	Uncertain
977[a]	FP	$1157.0^{+88.9}_{-72.6}$	1.25	1.10	0.095 ± 0.074	1.32 ± 1.04	CPM	CPM
980[a]	FP	$874.2^{+11.9}_{-14.1}$	2.00	1.26	0.088 ± 0.045	1.90 ± 0.96	CPM	Uncertain
984[a]	PC	$230.5^{+0.7}_{-0.6}$	0.79	0.73	0.072 ± 0.028	0.47 ± 0.19	CPM	CPM?
1119[a]	FP	117.4 ± 0.4	0.81	0.34	0.135 ± 0.026	0.79 ± 0.16	CPM	CPM
1150	Kepler-780	$2620.3^{+2699.0}_{-970.3}$	0.91	(0.67)	0.139 ± 0.063	24.68 ± 21.70	Uncertain	Uncertain
1531	Kepler-884	$325.1^{+17.6}_{-21.0}$	0.95	0.67	0.044 ± 0.091	0.37 ± 0.76	CPM	CPM
1613[a]	Kepler-907	$610.9^{+192.2}_{-151.0}$	1.19	0.87	0.049 ± 0.012	1.02 ± 0.45	CPM	CPM
1792AB[a]	Kepler-953	$705.0^{+50.4}_{-43.6}$	0.86	(0.67)	1.166 ± 0.062	84.38 ± 13.19	LOS	LOS
1792AC[a]	Kepler-953	$705.0^{+50.4}_{-43.6}$	0.86	(0.77)	1.274 ± 0.059	168.59 ± 23.37	LOS	LOS
1890[a]	Kepler-1002	$493.5^{+32.8}_{-34.5}$	1.12	0.67	0.084 ± 0.018	1.39 ± 0.33	CPM	CPM
1962[a]	PC	$1171.2^{+894.2}_{-382.9}$	1.05	1.02	0.084 ± 0.014	2.09 ± 1.18	CPM	Uncertain
2059	Kepler-1076	$411.2^{+113.8}_{-63.6}$	0.75	0.69	0.198 ± 0.060	1.57 ± 0.62	CPM	CPM?
2754[a,d]	Kepler-1339	$345.7^{+2.7}_{-2.4}$	1.00	(0.61)	0.053 ± 0.010	0.93 ± 0.18	CPM	CPM
2837	Kepler-1364	$1024.4^{+110.5}_{-94.2}$	1.55	(1.48)	0.871 ± 0.296	6.81 ± 2.50	LOS	Uncertain
2904	Kepler-1382	$826.3^{+23.9}_{-20.8}$	1.00	(0.63)	0.372 ± 0.174	8.06 ± 3.80	Uncertain	Uncertain
3020	PC	$1804.8^{+448.8}_{-324.6}$	0.83	(0.54)	0.510 ± 0.694	10.56 ± 14.73	Uncertain	Uncertain
3156[a]	FP	$119.8^{+1.0}_{-1.2}$	1.52	(0.72)	0.343 ± 0.038	0.63 ± 0.07	Uncertain	Uncertain
3214AB[a]	PC	$513.0^{+130.9}_{-82.3}$	1.05	0.78	0.068 ± 0.053	0.66 ± 0.54	CPM	CPM?
3214AC[a]	PC	$513.0^{+130.9}_{-82.3}$	1.05	0.69	0.182 ± 0.159	2.96 ± 2.67	CPM?	Uncertain
4287[a]	PC	$405.1^{+11.0}_{-10.9}$	1.12	0.79	0.036 ± 0.006	1.11 ± 0.19	CPM	CPM
5578[a]	PC	$300.6^{+30.3}_{-27.0}$	0.92	0.72	0.136 ± 0.008	1.05 ± 0.19	CPM	CPM
5822[a]	PC	145.9 ± 15.8	0.74	0.70	0.042 ± 0.024	0.21 ± 0.12	CPM	CPM

[a]Targets that have been observed with DSSI at APO.

[b] M_2 is calculated assuming the components are at the same distance, so the value is listed in parentheses if the system is not considered to be CPM.

[c]This column contains the dispositions previously reported in Colton et al. (2021) for comparison.

[d]KOI-2754 has only one observation at APO, which was found to be low SNR, resulting in a poor fit. The R_1, R_2, and disposition reported here were acquired via image plane measurements, an alternate method to power spectrum fitting (see 4.4.4 for further discussion).

Table 3. Improvement in uncertainties of R_1 and R_2

Data used in R_1 and R_2	Targets observed at APO[a] Med δR_1	Med δR_2	Targets not observed at APO[b] Med δR_1	Med δR_2
Colton et al. (2021)	0.08573	0.88600	0.10256	2.00920
+ *Gaia* DR3	0.08562	0.79477	0.07703	1.67044
+ DR3 and APO[c]	0.03344	0.40765	-	-

NOTE—This table presents median values in δR_1 and δR_2 for two different subsets of our target list. The first line of this table gives the median values across δR_1 and δR_2 in each set when calculated using only the data available in the Colton et al. (2021) paper, which drew system proper motions (μ_1) and parallaxes (π) from *Gaia* DR2. The second line gives the median values after updating μ_1 and π with *Gaia* DR3. The third line gives the median values after updating relative proper motions ($\Delta\mu$) and average separationa (ρ) with our APO data, in addition to the DR3 data.

[a] The subset of 27 KOIs that were observed at APO and have new relative proper motion data.

[b] The remaining subset of 10 KOIs that do not have new relative proper motion data from APO.

[c] KOI-2754 is excluded from these calculations due to the poor data point discussed in Section 4.4.4.

CPM. The effect of new speckle observations in addition to the DR3 data can be seen on the other six systems that changed disposition. Other than KOI-1962 (which lacks DR3 μ and π), we attribute the change in disposition of these systems to both APO and DR3 data; the effect that each source had on our results in general is analyzed further in the next section. Figure 6 illustrates two examples (discussed in Section 4.4) of the effect new speckle measurements have on calculating relative proper motion, with very different slopes of the best-fit lines (in arcsec yr^{-1}) before and after introducing the APO data.

4.2. *Improvement in Uncertainties in the Sample*

In Table 3, we examine how the new data improved the quality of our results overall. This table presents median values in δR_1 and δR_2 for two different subsets of our target list; we distinguish between the targets observed at APO and those not observed at APO to compare the improvement resulting from the *Gaia* DR3 data alone with the improvement from our new observations in addition to the DR3 data. We find that in the set of 10 targets which were not observed at APO, the median δR_1 value decreased by a factor of 1.33 and the median δR_2 value decreased by a factor of 1.20. In this case, the improvement is attributed entirely to the better data *Gaia* DR3 provides for measurements of μ and π over those of DR2 or the UCAC4 and Tycho-2 (Høg et al. 2000) catalogs. In the remaining set of 27 targets with new speckle observations at APO, we see the median δR_1 value decreases only slightly with the introduction of DR3 data, but is reduced by a factor of 2.56 with the APO data; the median δR_2 value decreases by a factor of 1.11 with the DR3 data and by a further factor of 1.95 with the APO data. Both sources are necessary for updating all of the system parameters utilized in this study; however, we see that adding new observational epochs of astrometric measurements tends to have a greater impact on reducing the uncertainty of our results, as our calculations of relative proper motion are made more robust with additional speckle data. This has resulted in improved dispositions for six systems, and it increases our overall confidence in the dispositions of targets that have remained the same from Colton et al. (2021).

4.3. *Distances to Resolved Systems*

A small subset of our targets were resolved in *Gaia* DR3 (Table 4). For each KOI in our sample, we searched the *Gaia* database for the positions and magnitudes of stars within a 5 arcsecond radius of the target's coordinates. If

Table 4. Distances to components resolved by *Gaia*

KOI no.	Disposition	R_p pc	R_s pc	$\bar{\rho}$ "	ρ_G "	$\overline{\Delta m}$ mag	Δm_G mag
13	CPM	$488.0^{+9.6}_{-8.4}$	$474.6^{+6.2}_{-5.3}$	1.1564	1.1558	0.73	0.19
118	LOS	$469.3^{+2.4}_{2.0}$	$1106.5^{+176.8}_{-158.4}$	1.4405	1.4860	4.78	4.56
120	Uncertain	$802.6^{+15.1}_{-12.3}$	$890.3^{+25.3}_{-27.6}$	1.5687	1.5661	1.03	0.49
284	CPM	$378.5^{+8.0}_{-6.7}$	$390.2^{+7.9}_{-7.3}$	0.8681	0.8668	0.77	0.36
980[a]	CPM	$874.2^{+11.9}_{-14.1}$	$859.8^{+38.0}_{-36.8}$	0.9343	0.9290	2.08	-
984	CPM	$230.5^{+0.7}_{-0.6}$	$234.0^{+1.0}_{-0.9}$	1.7542	1.7512	0.68	0.09
1792AC	LOS	$705.0^{+50.4}_{-43.6}$	$1332.1^{+55.3}_{-51.9}$	1.8935	1.8895	3.00[b]	0.76
3156	Uncertain	$119.8^{+1.0}_{-1.2}$	118.6 ± 0.5	1.1262	1.1372	2.27	1.92
3214AC	CPM?	$513.0^{+130.9}_{-82.3}$	$692.9^{+31.9}_{-28.7}$	1.2993	1.2986	2.97	2.78

Note—This table gives the Bailer-Jones distances to both primary (p) and secondary (s) components of nine different systems that were resolved in *Gaia* DR3. Also listed are the average separations and magnitude differences of all speckle measurements ($\bar{\rho}$ and $\overline{\Delta m}$) and the separation and magnitude difference derived from *Gaia* (ρ_G and Δm_G).

[a] The secondary component of KOI-980 does not have a reported magnitude in DR3, however, we still assume this to be the same component we observe due to the close match in separations.

[b] KOI-1792AC has a wide range of Δm measurements, from 5.03 to 0.86, all of which are flagged as upper limits in Table 5; this average may be skewed more significantly than other targets.

the separation and magnitude difference of the system aligned with the speckle measurements we have taken, it was assumed to be the same pair. For the two triple-component systems, KOI-1792 and KOI-3214, only one of the pairs is resolved in DR3. The separation and magnitude difference allow us to discern which component is being resolved; for example, KOI-1792AB has an average separation ~ 0.5, nearly a quarter that of the AC component, and KOI-3156AB has a $\overline{\Delta m} \sim 1.5$, roughly half that of the AC component. We notice that all $\overline{\Delta m}$ values in Table 4 are greater than the magnitude differences derived from *Gaia*'s measurements. It has been found that speckle Δm values tend to be higher than *Gaia* values when seeing $\times$ separation is greater than 0.6; because these systems have separations of $\sim$1 arcsec or greater, this will almost always be the case. This appears to be exacerbated in the $\overline{\Delta m}$ of KOI-1792AC, but we still believe we resolve the same pair because our separations are in close agreement, and the lower end of speckle Δm measurements aligns with *Gaia*'s.

Bailer-Jones (2023) provides a distance to each of the resolved components, giving us an independent method to compare against our derived dispositions; that is, we expect the components of any CPM system to have distances that overlap with one another, and any drastic difference between distances should correspond to a LOS system. Additionally, the similarity or disparity in distance to the components of any uncertain system can help to gauge the likelihood the system would appear as CPM or LOS with additional observations. There are three of these uncertain systems in Table 4: KOI-120, KOI-3156, and KOI-3214AC. We see that the distances for KOI-120 and KOI-3214AC are not in agreement, so it is likely they are both LOS doubles. However, the distances for KOI-3156 overlap with low relative errors ($\approx 0.5 - 1\%$), so it is still possible this system is gravitationally bound. Future speckle observations will help to determine if this system is in fact a CPM pair.

Interestingly, KOI-984 is considered to be CPM, but we notice its distances are not in agreement. This is because the distance uncertainties are very low on both stars, much lower than any other system. KOI-984 is also analyzed in Hirsch et al. (2017) with the isochrone-fitting method and reported as unbound. However, our analysis of the relative motion between its components over a twelve-year baseline indicates that the pair is indeed co-moving (see Figure 6

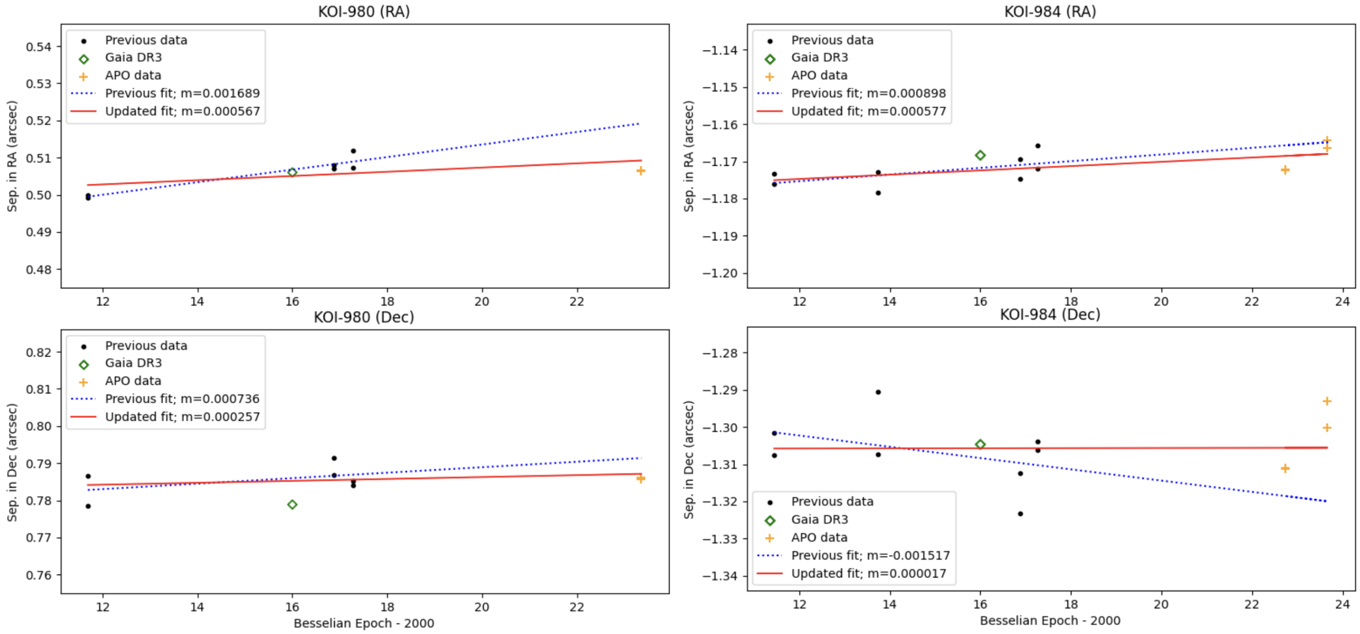

Figure 6. Separation in RA and Declination of KOI-980 and KOI-984, including best fit lines before and after the addition of data from APO. Both systems are resolved by *Gaia*, so we also plot the separations derived from the coordinates of each component given in DR3—note that the DR3 data point is *not* included in the calculation of either best fit line and is only plotted for reference.

and discussion in Section 4.4.2). Because the difference in distance is in the range of 2–5 pc, it is still possible this is a very widely separated binary system.

4.4. *Discussion of Specific Systems*

There are five targets that we look into in more detail to show more fully the extent to which new data from APO changes our analysis of double star systems. Three of these have changed disposition to CPM, one of which could be displaying orbital motion. The other two systems have undergone reanalysis following the discovery of poor data points that affected our interpretation of the relative motions.

4.4.1. *KOI-980*

KOI-980 changed disposition from Uncertain to CPM. Adding speckle data points to the plots in Figure 6 refines the measurement of $|\Delta\mu|$, which contributes to the calculation of both R_1 and R_2: New observations also affect the calculation of average separation used in R_2. In Colton et al. (2021), this system has $R_{2,prev} = 12.32 \pm 3.44$ and is now found to have $R_{2,new} = 1.90 \pm 0.96$. The DR3 data reduce this ratio by roughly a factor of two with a greater parallax than was given in DR2. The rest of the change is a result of the smaller average separation (primarily seen in the RA component) and the significantly reduced $|\Delta\mu|$, lowering both R_1 and R_2 by roughly a factor of three. We are further able to support its disposition as a CPM pair by comparing the distances to its components (Table 4).

4.4.2. *KOI-984*

KOI-984 changed disposition from CPM? to CPM. This was effected similarly to the change in KOI-980, although its R_2 value was not as dramatically affected by the updated parallax in DR3, nor did it previously exceed the CPM threshold. The significant shift in $|\Delta\mu|$ that reduced the system's R_1 value by a factor of three—and was thus the primary driver behind the new disposition—can be seen in Figure 6. Looking at its declination component, we notice that the previous fit was being driven by the wide spread in measurements between the 562 nm and 832 nm filters in the observation near the end of 2016. This could be caused by the system's wide separation (~1.8 arcseconds), nearly double that of KOI-980, for example. The APO data are more consistent with the other three observations of this system, indicating that the secondary star has not continued to drift apart from the primary as predicted by the previous fit. The new fit is also in better agreement with the separation from *Gaia* DR3. This target has one of the

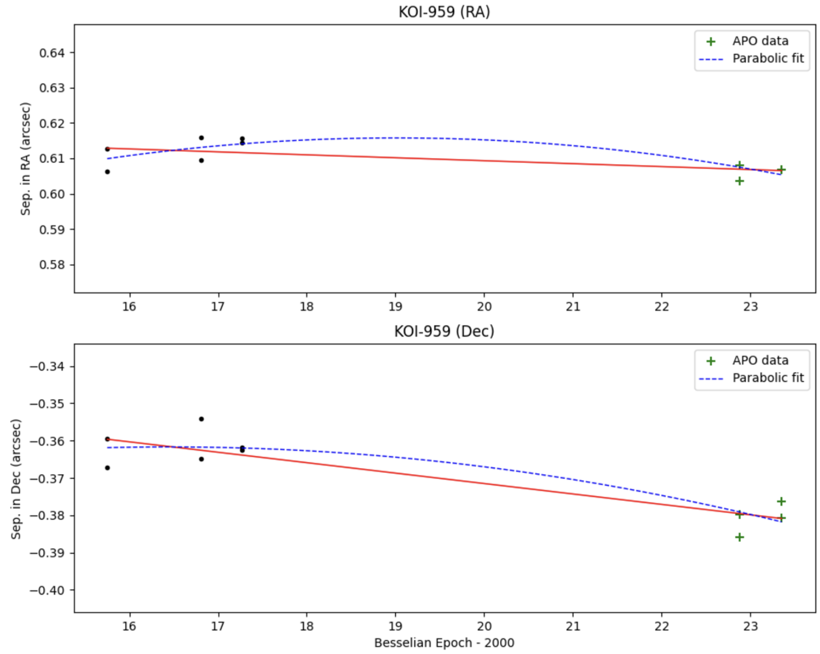

Figure 7. Separation versus time in RA and Declination of KOI-959, including both a linear and parabolic fit, demonstrating the possibility that this system is displaying orbital motion.

longest baselines of observations in our sample, having been nearly doubled since the previous analysis of Colton et al. (2021). This greatly increases our confidence that the components are exhibiting CPM.

4.4.3. *KOI-959*

KOI-959 has changed disposition from Uncertain to CPM. As noted in Colton et al. (2021), it was previously Uncertain because there was no parallax recorded in the literature, preventing the calculation of an R_2 value. The previous R_1 value indicated it was likely to be a CPM pair, and we confirm this with new observations from APO plus the system proper motion and parallax given in DR3. Additionally, it appears likely that KOI-959 is displaying orbital motion. The system is very nearby at 35.4 pc with an average angular separation of 0.713 arcseconds, corresponding to a physical separation of 25.2 AU (assuming the components are coplanar). From Kepler's third law, we expect the orbital period to be on the order of $a^{3/2} = (25.2)^{3/2} \approx 130$ years. Our observational baseline for this system is about eight years, roughly 6% of its orbital period, a significant enough fraction that it is possible to observe non-linear relative motion. In Figure 7, we overlay the linear fits to the separation versus time plots of KOI-959 with polynomial, parabolic fits and observe that the parabolas provide a slightly better fit to our data. New observations of this system, even as soon as late 2024 or early 2025, will provide strong leverage in determining which prediction more accurately represents this system's relative motion.

4.4.4. *KOI-2754*

We report KOI-2754 as remaining classified as a CPM system. However, it was reanalyzed after the initial calculations due to a poor data point from APO. When first analyzing this system, its disposition changed to Uncertain and the error in $\Delta\mu_\alpha$ and $\Delta\mu_\delta$ rose. The new APO observation did not appear consistent with previous measurements when plotting separation versus time, as shown by the "low SNR" point and previous fit in Figure 8. Upon investigation, we noticed that the power spectra had a low signal-to-noise ratio (SNR) and greater uncertainties than usual; the reduction code was also unable to fit the data from camera A (692 nm), and we concluded that this point should not be included in the calculation of $|\Delta\mu|$. Although the method of fitting the power spectrum does not work as well in this case, the secondary star, separated from the primary by $\sim$0.8 arcsec, is clearly visible in the reconstructed images from both cameras (these are shown in Figure 3), and we can measure the separation and position angle relative to the primary in the image plane as an alternative method, with uncertainties on the order of $\pm$10-15 mas (Horch, private communications). The results of this analysis are demonstrated in Figure 8 by the "new fit" line and the data points labeled "image measurements". This method produces measurements much more consistent with the five

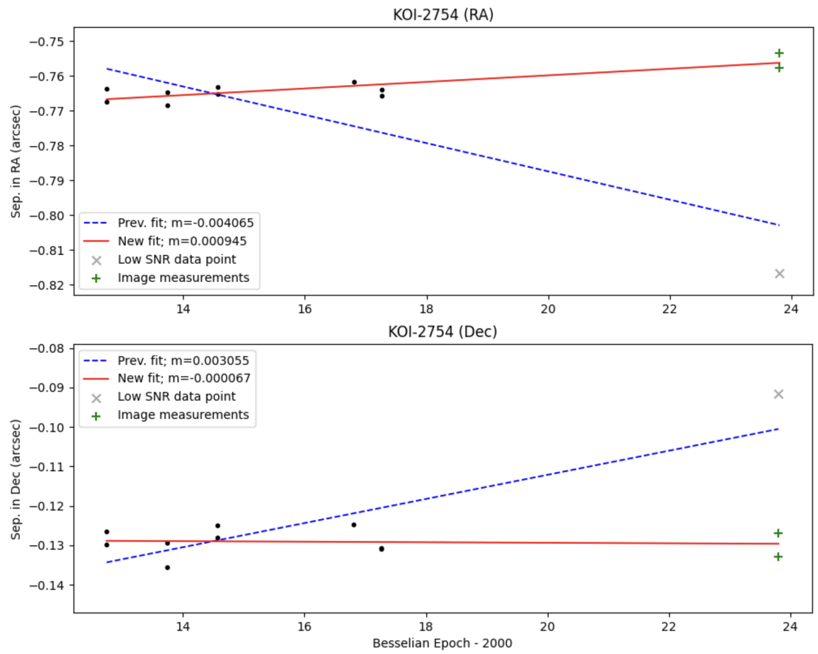

Figure 8. Plots of separation in RA and declination over time for KOI-2754. The low SNR data point is the result of fitting the power spectrum from camera B only. The image measurements are the result of fitting ρ and θ in the reconstructed image plane. The previous fit (blue dashed line) includes the low SNR data point but not the image measurements, while the new fit (red solid line) includes the image measurements and not the low SNR point. Because it is more consistent with previous data, we report the $\Delta\mu_\alpha$ and $\Delta\mu_\delta$ values from the new fit in Table 1 and use them in calculation of R_1 and R_2, as well as our determination of system disposition.

previous observations; however, it introduces greater uncertainties and differs from the method used in reducing the other speckle observations.

4.4.5. *KOI-1613*

Finally, KOI-1613 has also remained classified as a CPM system, and was thought to display orbital motion in the analysis of Davidson et al. (2024) following the first year of DSSI observations at APO in 2022. However, a second observation of this system was taken in 2023 that appeared inconsistent with the one from the previous year, prompting reanalysis. The previous data were found to be lower SNR and were refit by comparing against a different point source; this provided a better quality fit that was more consistent with earlier measurements. The results we present here use the reanalyzed data from 2022 in addition to the 2023 data and do not indicate orbital motion in the system.

5. CONCLUSION AND FUTURE WORK

We have provided an update to the relative astrometry of 37 *Kepler* Objects of Interest, performing the analysis demonstrated by Colton et al. (2021) after introducing new speckle data from observations taken with DSSI at APO in 2022 and 2023, as well as updated system parameters from *Gaia* DR3. Reanalyzing these systems with a baseline of observational data of up to 13 years, we report dispositions of these targets as either common proper motion pairs or line-of-sight doubles with greater confidence. Additionally, we report that eight of the systems have improved disposition in this new analysis; in summary, seven are now considered CPM and one is LOS. In total, we find 25 systems to be CPM or probable-CPM, five systems to be LOS companions, and seven remain uncertain.

APO data have been collected on 27 of the 37 KOIs. We are unable to observe some of the original sample at APO because the ARC 3.5 m telescope is limited to observing stars ∼13th magnitude or brighter, and some of our targets are fainter than this limit. We hope to make use of the 'Alopeke speckle imager at the Gemini-North 8.1 m telescope (Scott et al. 2021) to obtain new measurements of fainter systems in our sample. Looking further ahead, a similar analysis as presented here could be performed on systems beyond the *Kepler* surveys, such as the stars cataloged by the Transiting Exoplanet Survey Satellite (TESS); in general, these tend to be at closer distances to us compared to the systems in the Kepler field, making it easier to determine their relative motions over shorter timescales and more likely that we might observe orbital motion.

Although the APO observations have already improved our knowledge of the relative motions of 27 KOIs, many of them have only been observed there once, often representing the only measurement taken of the system over the last four to six years (e.g., KOI-2754), and their analysis would benefit from additional epochs being acquired. Additionally, there are 20 systems in Table 5 that were observed in Colton et al. (2021) but are not analyzed due to an insufficient number of independent observations (less than three). A number of these systems were observed with DSSI at APO in November of 2024—but not yet fully reduced—and these new observations will allow a disposition to be assigned for the first time. Finally, there are a handful of systems that still have a short total baseline (3–4 years), despite being observed at three or more independent epochs; we encourage further measurements of these to be taken as this will greatly benefit their analysis, as we found in the improved dispositions of six systems and the decreased overall uncertainties resulting from the new speckle data we have presented.

I am very grateful to both of my advisors, Jimmy Davidson and Steven Majewski, for their help and guidance in all aspects of my work on this thesis. I also extend special thanks to Elliott Horch for his work on reducing all of the speckle data presented here. Thank you to the staff at APO for providing on-sight housing during my visit, and I acknowledge support from The Research Corporation via a Cottrell Singular Exceptional Endeavors of Discovery (SEED) Award (Steve Majewski, PI).

This research presents results from the *Gaia* mission launched by the European Space Agency (ESA). Gaia data are being processed by the Gaia Data Processing and Analysis Consortium (DPAC). Funding for the DPAC is provided by national institutions, in particular the institutions participating in the Gaia MultiLateral Agreement (MLA). The Gaia mission website is https://www.cosmos.esa.int/gaia. The Gaia archive website is https://archives.esac.esa.int/gaia.

This research has made use of the Washington Double Star Catalog maintained at the U.S. Naval Observatory, the SIMBAD database operated at CDS, Strasbourg, France, as well as the Exoplanet Follow-up Observation Program (ExoFOP; NExScI 2022) website, operated by the California Institute of Technology, under contract with the National Aeronautics and Space Administration (NASA) under the Exoplanet Exploration Program.

REFERENCES

Bailer-Jones, C. A. L. 2023, AJ, 166, 269, doi: 10.3847/1538-3881/ad08bb

Bailer-Jones, C. A. L., Rybizki, J., Fouesneau, M., Mantelet, G., & Andrae, R. 2018, VizieR Online Data Catalog: Distances to 1.33 billion stars in Gaia DR2 (Bailer-Jones+, 2018), VizieR On-line Data Catalog: I/347. Originally published in: 2018AJ....156...58B

Charbonneau, D., Brown, T. M., Latham, D. W., & Mayor, M. 2000, ApJL, 529, L45, doi: 10.1086/312457

Ciardi, D. R., Beichman, C. A., Horch, E. P., & Howell, S. B. 2015, ApJ, 805, 16, doi: 10.1088/0004-637X/805/1/16

Colton, N. M., Horch, E. P., Everett, M. E., et al. 2021, AJ, 161, 21, doi: 10.3847/1538-3881/abc9af

Davidson, J. W., Horch, E. P., Majewski, S. R., et al. 2024, AJ, 167, 117, doi: 10.3847/1538-3881/ad1ff6

Deeg, H. J., & Alonso, R. 2018, in Handbook of Exoplanets, ed. H. J. Deeg & J. A. Belmonte, 117, doi: 10.1007/978-3-319-55333-7_117

Everett, M. E., Barclay, T., Ciardi, D. R., et al. 2015, AJ, 149, 55, doi: 10.1088/0004-6256/149/2/55

Gaia Collaboration, Brown, A. G. A., Vallenari, A., et al. 2018, A&A, 616, A1, doi: 10.1051/0004-6361/201833051

Gaia Collaboration, Arenou, F., Babusiaux, C., et al. 2023, A&A, 674, A34, doi: 10.1051/0004-6361/202243782

Henry, G. W., Marcy, G. W., Butler, R. P., & Vogt, S. S. 2000, ApJL, 529, L41, doi: 10.1086/312458

Hirsch, L. A., Ciardi, D. R., Howard, A. W., et al. 2017, AJ, 153, 117, doi: 10.3847/1538-3881/153/3/117

Hoffmann, M. 2000, Senior thesis, Rochester Institute of Technology. https://repository.rit.edu/theses/6785

Høg, E., Fabricius, C., Makarov, V. V., et al. 2000, A&A, 355, L27

Horch, E. P., Gomez, S. C., Sherry, W. H., et al. 2011, AJ, 141, 45, doi: 10.1088/0004-6256/141/2/45

Horch, E. P., Veillette, D. R., Baena Gallé, R., et al. 2009, AJ, 137, 5057, doi: 10.1088/0004-6256/137/6/5057

Horch, E. P., Broderick, K. G., Casetti-Dinescu, D. I., et al. 2021, AJ, 161, 295, doi: 10.3847/1538-3881/abf9a8

Mayor, M., & Queloz, D. 1995, Nature, 378, 355, doi: 10.1038/378355a0

Meng, J., Aitken, G. J. M., Hege, E. K., & Morgan, J. S. 1990, J. Opt. Soc. Am. A, 7, 1243, doi: 10.1364/JOSAA.7.001243

NExScI. 2022, Exoplanet Follow-up Observing Program Web Service, IPAC, doi: 10.26134/EXOFOP5

Scott, N. J., Howell, S. B., Horch, E. P., & Everett, M. E. 2018, PASP, 130, 054502, doi: 10.1088/1538-3873/aab484

Scott, N. J., Howell, S. B., Gnilka, C. L., et al. 2021, Frontiers in Astronomy and Space Sciences, 8, 138, doi: 10.3389/fspas.2021.716560

Smith, B. A., & Terrile, R. J. 1984, Science, 226, 1421, doi: 10.1126/science.226.4681.1421

Wolszczan, A., & Frail, D. A. 1992, Nature, 355, 145, doi: 10.1038/355145a0

Youdin, A. N. 2011, ApJ, 742, 38, doi: 10.1088/0004-637X/742/1/38

Zacharias, N., Finch, C. T., Girard, T. M., et al. 2013, AJ, 145, 44, doi: 10.1088/0004-6256/145/2/44

APPENDIX

A. ALL SPECKLE OBSERVATIONS TO DATE

This table contains all speckle data collected thus far, combining the measurements reported in Colton et al. (2021) with our more recent APO data. For each observation, we list 1) KOI number, 2) Kepler system number (if available), 3) Washington Double Star number, 4) epoch of observation, 5) position angle, 6) separation, 7) magnitude difference, 8) filter wavelength, 9) filter FWHM, and 10) notes on the specific observation. For observations at APO, the astrometric precision was measured to be 2.06 ± 0.11 mas and the photometric precision was 0.14 ± 0.04 mag (Davidson et al. 2024). However, the uncertainty in separation and magnitude difference is characterized in general by taking the standard error from the mean of each observation.

Table 5. KOI Speckle Measurements

KOI no.	Exoplanet system	WDS	Date (2000+)	θ (°)	ρ (")	Δm (mag)	λ (nm)	$\Delta\lambda$ (nm)	Tel., Inst., and notes[c]
1	Kepler-1	19072+4919	11.448	136.7	1.106	<4.75	692	40	WD,a
1	Kepler-1	19072+4919	11.448	136	1.1055	<3.49	880	50	WD,a
1	Kepler-1	19072+4919	13.7227	135	1.1016	<4.4	692	40	WD,a
1	Kepler-1	19072+4919	13.7227	136.5	1.1024	<3.26	880	50	WD,a
1	Kepler-1	19072+4919	13.7284	136.4	1.1107	<4.25	692	40	WD,a
1	Kepler-1	19072+4919	13.7284	136.3	1.1093	<3.41	880	50	WD,a
1	Kepler-1	19072+4919	17.2747	136.2	1.1101	<3.45	832	40	WN,a
1	Kepler-1	19072+4919	17.2747	136.2	1.111	<4.95	562	44	WN,a
1	Kepler-1	19072+4919	22.7441	136.1	1.1192	<3.86	692	40	AD,a
1	Kepler-1	19072+4919	22.7441	136.5	1.1241	<3.04	880	50	AD,a
13	Kepler-13	19079+4652	10.4649	279.7	1.1647	<0.84	692	40	WD,a
13	Kepler-13	19079+4652	10.4732	279.8	1.1619	<0.9	692	40	WD,a
13	Kepler-13	19079+4652	10.4732	279.6	1.1667	<1.2	562	44	WD,a
13	Kepler-13	19079+4652	11.4423	280.2	1.1578	<0.92	692	40	WD,a
13	Kepler-13	19079+4652	11.4423	280.1	1.1613	<0.65	880	50	WD,a
13	Kepler-13	19079+4652	11.6832	279.6	1.1587	<0.73	692	40	WD,a
13	Kepler-13	19079+4652	11.6832	279.7	1.1591	<0.57	880	50	WD,a
13	Kepler-13	19079+4652	12.7397	279.7	1.1494	<0.07	692	40	WD,a
13	Kepler-13	19079+4652	12.7397	279.2	1.1474	<1.56	880	50	WD,a
13	Kepler-13	19079+4652	13.4056	279.6	1.1578	<0.62	692	40	WD,a
13	Kepler-13	19079+4652	13.4056	279.6	1.1526	<0.58	880	50	WD,a
13	Kepler-13	19079+4652	13.7227	280.1	1.1546	<0.04	692	40	WD,a
13	Kepler-13	19079+4652	13.7227	280.1	1.1534	<0.28	880	50	WD,a
13	Kepler-13	19079+4652	13.7284	279.9	1.1627	<0.95	692	40	WD,a
13	Kepler-13	19079+4652	13.7284	280	1.1589	<0.81	880	50	WD,a
13	Kepler-13	19079+4652	14.2192	280.2	1.1476	<0.65	692	40	LD,a
13	Kepler-13	19079+4652	14.2192	280.5	1.1435	<0.55	880	50	LD,a
13	Kepler-13	19079+4652	14.564	280	1.1554	<0.71	692	40	GD,a
13	Kepler-13	19079+4652	14.564	280.3	1.1554	0.77	880	50	GD
13	Kepler-13	19079+4652	14.7493	279.6	1.1532	<0.87	692	40	LD,a
13	Kepler-13	19079+4652	14.7493	279.8	1.1535	<0.61	880	50	LD,a
13	Kepler-13	19079+4652	16.8548	279.9	1.1553	<0.63	832	40	WN,a,b
13	Kepler-13	19079+4652	16.8548	279.8	1.1618	<1	562	44	WN,a,b
13	Kepler-13	19079+4652	17.2718	279.8	1.1557	<0.69	832	40	WN,a

Table 5. KOI Speckle Measurements

KOI no.	Exoplanet system	WDS	Date (2000+)	θ (°)	ρ (")	Δm (mag)	λ (nm)	$\Delta\lambda$ (nm)	Tel., Inst., and notes[c]
13	Kepler-13	19079+4652	17.2718	279.8	1.1552	<1.04	562	44	WN,a
13	Kepler-13	19079+4652	22.867	279.9	1.16	<0.63	692	40	AD,a
13	Kepler-13	19079+4652	22.867	279.7	1.1603	<0.27	880	50	AD,a
68		18476+4450	10.4703	256.6	0.7302	2.85	692	40	WD
68		18476+4450	10.4703	257	0.7317	<3.31	562	44	WD,a
98	Kepler-14	19108+4720	10.465	143.9	0.2916	0.71	692	40	WD
98	Kepler-14	19108+4720	10.465	143.7	0.2899	0.46	562	44	WD
98	Kepler-14	19108+4720	10.7164	143.9	0.2896	0.45	692	40	WD
98	Kepler-14	19108+4720	10.7164	144	0.2911	0.47	562	44	WD
98	Kepler-14	19108+4720	10.7195	144	0.2894	0.87	692	40	WD
98	Kepler-14	19108+4720	10.7195	143.6	0.2897	0.91	562	44	WD
98	Kepler-14	19108+4720	10.8096	144.5	0.2883	0.59	692	40	WD
98	Kepler-14	19108+4720	10.8096	143.9	0.288	0.58	880	50	WD
98	Kepler-14	19108+4720	10.8121	144.2	0.2871	0.59	692	40	WD
98	Kepler-14	19108+4720	10.8121	143.9	0.2858	0.04	880	50	WD
98	Kepler-14	19108+4720	10.8148	145.3	0.2872	1.81	692	40	WD
98	Kepler-14	19108+4720	10.8148	143.2	0.2884	0	880	50	WD
98	Kepler-14	19108+4720	11.4424	144.6	0.2887	0.45	692	40	WD
98	Kepler-14	19108+4720	11.4424	144.2	0.2876	0.61	880	50	WD
98	Kepler-14	19108+4720	11.6832	143.8	0.2888	1.07	692	40	WD
98	Kepler-14	19108+4720	11.6832	143.8	0.2949	0.49	880	50	WD
98	Kepler-14	19108+4720	12.5708	144.4	0.2893	<0.44	692	40	WD,a
98	Kepler-14	19108+4720	12.5708	144.5	0.2901	<1.09	692	40	WD,a
98	Kepler-14	19108+4720	12.7397	143.9	0.278	2.19	692	40	WD
98	Kepler-14	19108+4720	12.7397	147.1	0.2757	1.66	880	50	WD
98	Kepler-14	19108+4720	13.4056	144	0.2877	0.42	692	40	WD
98	Kepler-14	19108+4720	13.4056	143.9	0.2905	0.5	880	50	WD
98	Kepler-14	19108+4720	13.7227	143.9	0.2904	0.34	692	40	WD
98	Kepler-14	19108+4720	13.7227	143.8	0.2856	0.45	880	50	WD
98	Kepler-14	19108+4720	13.7282	145.4	0.2925	0.66	692	40	WD
98	Kepler-14	19108+4720	13.7282	145	0.2836	0.44	880	50	WD
98	Kepler-14	19108+4720	14.2192	145.1	0.2897	0.04	692	40	LD
98	Kepler-14	19108+4720	14.2192	144.5	0.2894	0.65	880	50	LD
98	Kepler-14	19108+4720	14.564	144.4	0.2877	0.38	692	40	GD
98	Kepler-14	19108+4720	14.564	144.7	0.2888	0.38	880	50	GD
98	Kepler-14	19108+4720	14.7493	144.5	0.2885	0.45	692	40	LD
98	Kepler-14	19108+4720	14.7493	144.1	0.2874	0.55	880	50	LD
98	Kepler-14	19108+4720	16.8054	144.6	0.2854	0.04	832	40	WN
98	Kepler-14	19108+4720	16.8054	144.9	0.2763	1.03	562	44	WN,b
98	Kepler-14	19108+4720	17.3892	144.2	0.2854	0.39	832	40	WN,b
98	Kepler-14	19108+4720	17.3892	144.5	0.2851	0.25	562	44	WN,b
98	Kepler-14	19108+4720	23.8009	144.7	0.2852	0.08	692	40	AD
98	Kepler-14	19108+4720	23.8009	144	0.2791	0.01	880	50	AD
112	Kepler-466	19426+4830	14.5588	115.2	0.1029	1.76	692	40	GD
112	Kepler-466	19426+4830	14.5588	116.1	0.102	1.61	880	50	GD
112	Kepler-466	19426+4830	17.3596	105	0.0851	1.02	832	40	WN

Table 5. KOI Speckle Measurements

KOI no.	Exoplanet system	WDS	Date (2000+)	θ (°)	ρ (")	Δm (mag)	λ (nm)	$\Delta\lambda$ (nm)	Tel., Inst., and notes[c]
112	Kepler-466	19426+4830	17.3596	107.1	0.0925	1.2	562	44	WN
113		19291+3740	10.7165	166.8	0.1769	1.59	692	40	WD
113		19291+3740	10.7165	165.7	0.1789	1.79	562	44	WD
118	Kepler-467	19095+3839	11.4483	214.5	1.2795	<5.01	692	40	WD,a
118	Kepler-467	19095+3839	14.5642	212.9	1.423	<5.07	692	40	GD,a
118	Kepler-467	19095+3839	14.5642	213.3	1.4231	<4.34	880	50	GD,a
118	Kepler-467	19095+3839	17.1899	212.3	1.5405	<4.52	832	40	WN,a
118	Kepler-467	19095+3839	17.1899	212.1	1.5363	<4.95	562	44	WN,a
120		19376+5010	15.8118	129.1	1.5662	<1.5	880	50	WD,a,b
120		19376+5010	16.8031	130.1	1.5593	<1.13	832	40	WN,a
120		19376+5010	17.2637	129.5	1.5655	<0.68	832	40	WN,a
120		19376+5010	17.2637	129.6	1.5634	<0.81	562	44	WN,a
120		19376+5010	22.7441	129.5	1.5724	<0.94	692	40	AD,a
120		19376+5010	22.7441	129.4	1.5759	<1.1	880	50	AD,a
120		19376+5010	22.8753	129.8	1.574	<0.86	692	40	AD,a
120		19376+5010	22.8753	129.6	1.573	<0.51	880	50	AD,a
177		19527+4214	11.4537	218	0.2288	0.61	692	40	WD
177		19527+4214	11.4537	217.6	0.2304	0.36	880	50	WD
177		19527+4214	13.7286	217.3	0.2281	0.83	692	40	WD,b
177		19527+4214	13.7286	217.4	0.2266	0.81	880	50	WD,b
177		19527+4214	17.2775	217.1	0.2257	0.19	832	40	WN
177		19527+4214	17.2775	217.2	0.226	0.43	562	44	WN
190		18586+4101	11.6886	109.1	0.1864	1.23	692	40	WD
190		18586+4101	13.7308	290.8	0.1505	1.08	692	40	WD
258AB		18582+4858	10.7169	73.2	1.0136	<3.64	692	40	WD,a
258AB		18582+4858	10.7169	72.4	1.007	<3.59	562	44	WD,a
258AB		18582+4858	13.7227	73.2	1.027	<3.21	692	40	WD,a
258AB		18582+4858	13.7227	73.1	1.0203	<2.88	880	50	WD,a
258AB		18582+4858	13.7284	73.1	1.0258	<3.12	692	40	WD,a
258AB		18582+4858	13.7284	73.2	1.0215	3.1	880	50	WD
258AB		18582+4858	17.2719	72.6	1.0202	<2.95	832	40	WN,a
258AB		18582+4858	17.2719	72.6	1.0194	<3.48	562	44	WN,a
258AB		18582+4858	23.6669	72.8	1.0384	<3.02	692	40	AD,a
258AB		18582+4858	23.6669	72.6	1.0347	<2.92	880	50	AD,a
258AC		18582+4858	13.7227	74.4	1.4663	<5.07	692	40	WD,a
258AC		18582+4858	13.7227	75.4	1.474	<4.5	880	50	WD,a
258AC		18582+4858	13.7284	73.9	1.4731	<5.89	692	40	WD,a
258AC		18582+4858	13.7284	74.6	1.4698	<4.66	880	50	WD,a
258AC		18582+4858	17.2719	74.4	1.4083	<4.24	832	40	WN,a
258AC		18582+4858	17.2719	74.8	1.417	<5.49	562	44	WN,a
258AC		18582+4858	23.6669	75	1.3743	<4.22	692	40	AD,a
258AC		18582+4858	23.6669	74.9	1.3786	<3.87	880	50	AD,a
270	Kepler-449	19349+4154	11.4481	64.1	0.1566	0.6	692	40	WD
270	Kepler-449	19349+4154	11.4481	63.8	0.1564	0.93	880	50	WD
270	Kepler-449	19349+4154	13.7283	63.8	0.1658	1.05	692	40	WD
270	Kepler-449	19349+4154	13.7283	63.4	0.1656	0.36	880	50	WD

Table 5. KOI Speckle Measurements

KOI no.	Exoplanet system	WDS	Date (2000+)	θ (°)	ρ (")	Δm (mag)	λ (nm)	$\Delta\lambda$ (nm)	Tel., Inst., and notes[c]
270	Kepler-449	19349+4154	14.5558	64.1	0.1647	0.73	692	40	GD
270	Kepler-449	19349+4154	14.5558	64.4	0.1647	0.87	880	50	GD
270	Kepler-449	19349+4154	16.8629	64.2	0.1706	0.56	832	40	WN
270	Kepler-449	19349+4154	16.8629	64.1	0.1709	0.58	562	44	WN
270	Kepler-449	19349+4154	17.2555	63.9	0.1723	0.54	832	40	WN
270	Kepler-449	19349+4154	17.2555	63.9	0.1731	0.57	562	44	WN
270	Kepler-449	19349+4154	22.744	64.8	0.1854	0.73	692	40	AD
270	Kepler-449	19349+4154	22.744	65.8	0.1838	0.69	880	50	AD
279	Kepler-450	19419+5101	11.4452	247.3	0.9089	<3.88	692	40	WD,*a*
279	Kepler-450	19419+5101	11.4452	247.2	0.9158	3	880	50	WD
279	Kepler-450	19419+5101	13.7284	247.2	0.922	3.61	692	40	WD
279	Kepler-450	19419+5101	13.7284	246.5	0.9218	3.02	880	50	WD
279	Kepler-450	19419+5101	14.5588	246.9	0.9145	<3.68	692	40	GD,*a*
279	Kepler-450	19419+5101	14.5588	247.1	0.9115	3.26	880	50	GD
279	Kepler-450	19419+5101	16.863	247	0.918	<3.23	832	40	WN,*a*
279	Kepler-450	19419+5101	16.863	247.3	0.9197	<4.14	562	44	WN,*a*
279	Kepler-450	19419+5101	17.2747	246.8	0.9156	<3.26	832	40	WN,*a*
279	Kepler-450	19419+5101	17.2747	246.7	0.9135	<4.04	562	44	WN,*a*
279	Kepler-450	19419+5101	22.8673	247.4	0.9159	<3.35	692	40	AD,*a*
279	Kepler-450	19419+5101	22.8673	248	0.9137	<3.12	880	50	AD,*a*
284	Kepler-132	18529+4121	10.4785	97.3	0.871	<1.12	692	40	WD,*a*
284	Kepler-132	18529+4121	10.4785	97.2	0.8732	<1.04	562	44	WD,*a*
284	Kepler-132	18529+4121	13.5644	97.4	0.8672	0.55	692	40	GD
284	Kepler-132	18529+4121	13.5644	97.3	0.8655	1.38	880	50	GD
284	Kepler-132	18529+4121	13.7282	97.3	0.8626	0.83	880	50	WD,*a*
284	Kepler-132	18529+4121	13.7283	97.5	0.8667	0.67	692	40	WD,*a*
284	Kepler-132	18529+4121	13.7308	97.5	0.8697	0.76	692	40	WD
284	Kepler-132	18529+4121	13.7308	97.8	0.8707	0.43	880	50	WD
284	Kepler-132	18529+4121	16.8028	98	0.8654	<0.36	832	40	WN,*a*
284	Kepler-132	18529+4121	16.8028	97.7	0.8752	<0.47	562	44	WN,*a*,*b*
284	Kepler-132	18529+4121	17.3702	97.5	0.8711	<0.83	832	40	WN,*a*,*b*
284	Kepler-132	18529+4121	17.3702	97.4	0.8677	<0.79	562	44	WN,*a*,*b*
284	Kepler-132	18529+4121	22.8754	97.7	0.8734	0.35	692	40	AD
284	Kepler-132	18529+4121	22.8754	97.3	0.8656	0.53	880	50	AD
284	Kepler-132	18529+4121	23.8008	97.8	0.8631	<0.62	692	40	AD,*a*
284	Kepler-132	18529+4121	23.8008	97.7	0.8609	<0.52	880	50	AD,*a*
287		19477+4451	10.7196	210.7	1.0734	<1.63	692	40	WD,*a*
287		19477+4451	10.7196	210.5	1.0726	<1.72	562	44	WD,*a*
287		19477+4451	16.8768	211.3	1.073	<0.76	832	40	WN,*a*,*b*
287		19477+4451	16.8768	211.2	1.0789	<1.08	562	44	WN,*a*
298	Kepler-515	19220+5203	17.2636	92.8	1.9963	<0.71	832	40	WN,*a*
300		19205+3831	10.7166	318.3	0.1663	1.87	692	40	WD
300		19205+3831	10.7166	317.4	0.1623	1.96	562	44	WD
307	Kepler-520	19327+4137	11.4508	248.3	0.08	0.56	692	40	WD
307	Kepler-520	19327+4137	11.4508	245.7	0.0792	0	880	50	WD,*b*
307	Kepler-520	19327+4137	14.5477	244.9	0.0766	0.33	692	40	GD

Table 5. KOI Speckle Measurements

KOI no.	Exoplanet system	WDS	Date (2000+)	θ (°)	ρ (")	Δm (mag)	λ (nm)	$\Delta\lambda$ (nm)	Tel., Inst., and notes[c]
307	Kepler-520	19327+4137	14.5477	244.7	0.076	0.25	880	50	GD
307	Kepler-520	19327+4137	16.8766	252.9	0.0723	0	832	40	WN
307	Kepler-520	19327+4137	16.8766	247.4	0.0721	0.25	562	44	WN
307	Kepler-520	19327+4137	17.2036	238.5	0.0616	0.75	832	40	WN,*b*
307	Kepler-520	19327+4137	17.2036	241.5	0.061	0	562	44	WN,*b*
379		19282+3747	11.4537	80.5	1.9158	<2.26	692	40	WD,*a*
379		19282+3747	11.4537	80.5	1.9208	<1.8	880	50	WD,*a*
640	Kepler-632	19490+4017	11.4564	301.3	0.4314	0.69	692	40	WD
640	Kepler-632	19490+4017	11.4564	301	0.4339	0.63	880	50	WD
640	Kepler-632	19490+4017	13.7286	301.4	0.4419	1.17	692	40	WD
640	Kepler-632	19490+4017	13.7286	300.7	0.4353	0.45	880	50	WD
640	Kepler-632	19490+4017	16.8003	301.5	0.4195	0.89	832	40	WN,*b*
640	Kepler-632	19490+4017	16.8003	299.2	0.4189	1.45	562	44	WN,*b*
640	Kepler-632	19490+4017	17.2774	300.9	0.4269	0.39	832	40	WN,*b*
640	Kepler-632	19490+4017	17.2774	300.9	0.4256	0.31	562	44	WN,*b*
959		19102+4657	15.7517	121.2	0.7089	<1.6	692	40	WD,*a*
959		19102+4657	15.7517	120.4	0.7105	<1.1	880	50	WD,*a*
959		19102+4657	16.8055	120.9	0.7103	<0.5	832	40	WN,*a*
959		19102+4657	16.8055	119.9	0.7105	<0.01	562	44	WN,*a*
959		19102+4657	17.2693	120.5	0.7145	0.59	832	40	WN,*b*
959		19102+4657	17.2693	120.5	0.7131	<0.68	562	44	WN,*a*
959		19102+4657	22.8754	122.6	0.7164	0.71	692	40	AD
959		19102+4657	22.8754	122	0.7169	0.65	880	50	AD
959		19102+4657	23.3526	122.1	0.7164	<0.64	692	40	AD,*a*
959		19102+4657	23.3526	121.8	0.714	0.47	880	50	AD
976		19238+3832	11.448	137	0.2575	0.62	692	40	WD
976		19238+3832	11.448	136.9	0.2561	0.65	880	50	WD
976		19238+3832	13.7228	136	0.2544	0.58	692	40	WD
976		19238+3832	13.7228	136.1	0.2537	0.53	880	50	WD
976		19238+3832	13.7283	135.9	0.255	0.58	692	40	WD
976		19238+3832	13.7283	135.9	0.2532	0.69	880	50	WD
976		19238+3832	16.8002	135.3	0.2504	0.74	832	40	WN,*b*
976		19238+3832	16.8002	134.3	0.25	0.79	562	44	WN
976		19238+3832	16.8741	134.9	0.2486	0.79	832	40	WN
976		19238+3832	16.8741	137.8	0.2436	0.71	562	44	WN
976		19238+3832	17.2117	134.9	0.2496	0.61	832	40	WN
976		19238+3832	17.2117	135	0.2493	0.73	562	44	WN
976		19238+3832	23.3526	132.8	0.2447	0.68	692	40	AD
976		19238+3832	23.3526	132.7	0.2458	0.61	880	50	AD
977		19309+4851	11.4481	349.5	0.3371	3.88	692	40	WD
977		19309+4851	11.4481	349.2	0.3377	4	880	50	WD
977		19309+4851	13.7227	349.2	0.3322	3.46	692	40	WD
977		19309+4851	13.7227	350.7	0.3285	4.2	880	50	WD
977		19309+4851	13.7284	349	0.3443	3.96	692	40	WD
977		19309+4851	16.8658	349.5	0.3401	4.08	832	40	WN
977		19309+4851	16.8658	350.2	0.3363	3.59	562	44	WN

Table 5. KOI Speckle Measurements

KOI no.	Exoplanet system	WDS	Date (2000+)	θ (°)	ρ (″)	Δm (mag)	λ (nm)	$\Delta\lambda$ (nm)	Tel., Inst., and notes[c]
977		19309+4851	17.2719	349.7	0.3344	4.37	832	40	WN
977		19309+4851	17.2719	348.9	0.3336	3.69	562	44	WN
977		19309+4851	22.8672	349.9	0.3363	4.1	692	40	AD
977		19309+4851	22.8672	350.4	0.3414	4.3	880	50	AD
980		19424+5043	11.6917	32.4	0.9317	<2.1	692	40	WD,*a*
980		19424+5043	11.6917	32.7	0.9252	<2.16	880	50	WD,*a*
980		19424+5043	16.8657	32.8	0.936	<1.68	832	40	WN,*a*
980		19424+5043	16.8657	32.7	0.9404	<2.21	562	44	WN,*a*
980		19424+5043	17.2719	32.9	0.9337	<1.81	832	40	WN,*a*
980		19424+5043	17.2719	33.1	0.9374	<2.51	562	44	WN,*a*
980		19424+5043	23.3526	32.8	0.9348	<1.93	692	40	AD,*a*
980		19424+5043	23.3526	32.8	0.9353	<1.66	880	50	AD,*a*
984		19242+3650	11.448	221.9	1.7569	<1.01	692	40	WD,*a*
984		19242+3650	11.448	222.1	1.7541	<0.7	880	50	WD,*a*
984		19242+3650	13.7283	221.9	1.7564	<1.01	692	40	WD,*a*
984		19242+3650	13.7283	222.4	1.7475	<0.65	880	50	WD,*a*
984		19242+3650	16.8767	221.7	1.7578	<0.55	832	40	WN,*a*
984		19242+3650	16.8767	221.6	1.7694	<0.77	562	44	WN,*a*
984		19242+3650	17.2556	221.8	1.749	<0.29	832	40	WN,*a*,*b*
984		19242+3650	17.2556	221.9	1.755	<0.49	562	44	WN,*a*
984		19242+3650	22.7441	221.8	1.759	<0.55	692	40	AD,*a*
984		19242+3650	22.7441	221.8	1.7588	<0.55	880	50	AD,*a*
984		19242+3650	23.6669	221.9	1.7467	<0.56	692	40	AD,*a*
984		19242+3650	23.6669	222	1.7401	0	880	50	AD,*a*
1119		19380+3812	15.7461	65.8	0.4835	4.09	692	40	WD
1119		19380+3812	15.7461	64.6	0.4851	3.15	880	50	WD
1119		19380+3812	16.8604	65.2	0.4915	<3.58	832	40	WN,*a*
1119		19380+3812	16.8767	65.7	0.4931	3.49	832	40	WN
1119		19380+3812	17.2117	65.6	0.4853	3.38	832	40	WN
1119		19380+3812	23.6698	67.7	0.4841	4.34	692	40	AD
1119		19380+3812	23.6698	70.5	0.4915	3.27	880	50	AD
1150	Kepler-780	18471+4418	11.4564	323.1	0.3986	1.85	692	40	WD
1150	Kepler-780	18471+4418	11.4564	325.4	0.3931	1.99	880	50	WD
1150	Kepler-780	18471+4418	16.8738	323.2	0.4065	1.33	832	40	WN
1150	Kepler-780	18471+4418	16.8738	322.5	0.4019	2.05	562	44	WN
1150	Kepler-780	18471+4418	17.1899	323	0.401	1.69	832	40	WN
1150	Kepler-780	18471+4418	17.1899	323	0.4013	2.06	562	44	WN
1463		19130+4323	11.4483	31	0.254	4.06	692	40	WD
1463		19130+4323	11.4483	31.5	0.2568	3.6	880	50	WD
1531	Kepler-884	19303+4955	11.4536	99	0.3672	2.25	692	40	WD
1531	Kepler-884	19303+4955	11.4536	98.1	0.3696	1.94	880	50	WD
1531	Kepler-884	19303+4955	13.7285	97	0.3762	2.34	692	40	WD
1531	Kepler-884	19303+4955	13.7285	96.2	0.3726	2.17	880	50	WD
1531	Kepler-884	19303+4955	17.2637	98.8	0.3664	1.87	832	40	WN
1531	Kepler-884	19303+4955	17.2637	98.8	0.3709	2.29	562	44	WN
1613	Kepler-907	19019+4138	11.448	185.1	0.2128	1.28	692	40	WD

Table 5. KOI Speckle Measurements

KOI no.	Exoplanet system	WDS	Date (2000+)	θ (°)	ρ (")	Δm (mag)	λ (nm)	$\Delta\lambda$ (nm)	Tel., Inst., and notes[c]
1613	Kepler-907	19019+4138	11.448	184.9	0.2157	1.22	880	50	WD
1613	Kepler-907	19019+4138	13.7226	184.7	0.218	1.49	692	40	WD
1613	Kepler-907	19019+4138	13.7226	183.9	0.2155	1.62	880	50	WD
1613	Kepler-907	19019+4138	13.7282	184.9	0.2037	1.25	692	40	WD
1613	Kepler-907	19019+4138	13.7282	183.4	0.2001	1.09	880	50	WD
1613	Kepler-907	19019+4138	16.8603	183.1	0.2084	1.1	832	40	WN
1613	Kepler-907	19019+4138	16.8603	183.1	0.2102	1.45	562	44	WN
1613	Kepler-907	19019+4138	16.8766	184.2	0.2067	1.29	832	40	WN
1613	Kepler-907	19019+4138	16.8766	184.4	0.2073	1.38	562	44	WN
1613	Kepler-907	19019+4138	17.2007	184.4	0.2043	1.25	832	40	WN
1613	Kepler-907	19019+4138	17.2007	184.4	0.2038	1.36	562	44	WN
1613	Kepler-907	19019+4138	22.744	185.5	0.1949	1.31	692	40	AD
1613	Kepler-907	19019+4138	22.744	188.6	0.1916	1.21	880	50	AD
1613	Kepler-907	19019+4138	23.6669	182.7	0.2034	1.29	692	40	AD
1613	Kepler-907	19019+4138	23.6669	184.3	0.1994	1.16	880	50	AD
1792AB	Kepler-953	19159+4437	11.6917	304.4	0.4909	2.1	692	40	WD
1792AB	Kepler-953	19159+4437	11.6917	305.4	0.4809	2.13	880	50	WD
1792AB	Kepler-953	19159+4437	15.7434	287.4	0.4893	2.42	692	40	WD
1792AB	Kepler-953	19159+4437	15.7434	288.3	0.4925	2.7	880	50	WD
1792AB	Kepler-953	19159+4437	16.8056	282.8	0.5003	2.06	832	40	WN
1792AB	Kepler-953	19159+4437	16.8056	282.9	0.5087	1.98	562	44	WN
1792AB	Kepler-953	19159+4437	23.801	260.1	0.6407	<2.25	692	40	AD,a
1792AB	Kepler-953	19159+4437	23.801	268	0.6482	<2.8	880	50	AD,a
1792AC	Kepler-953	19159+4437	11.6917	108.4	1.9237	<4.32	692	40	WD,a
1792AC	Kepler-953	19159+4437	11.6917	110.6	1.9377	<2.94	880	50	WD,a
1792AC	Kepler-953	19159+4437	15.7434	112.8	1.9171	<5.03	692	40	WD,a
1792AC	Kepler-953	19159+4437	15.7434	113.3	1.9052	<3.85	880	50	WD,a
1792AC	Kepler-953	19159+4437	16.8056	115.4	1.8805	<0.99	832	40	WN,a
1792AC	Kepler-953	19159+4437	16.8056	114.6	1.8931	<0.86	562	44	WN,a
1792AC	Kepler-953	19159+4437	23.801	123	1.8501	<1.33	692	40	AD,a
1792AC	Kepler-953	19159+4437	23.801	123	1.8403	<1.34	880	50	AD,a
1853	Kepler-983	19004+4500	13.7338	305.6	0.9663	<0.73	692	40	WD,a,b
1853	Kepler-983	19004+4500	17.2774	304.5	0.9577	0.42	832	40	WN,b
1853	Kepler-983	19004+4500	17.2774	304.6	0.9571	0.38	562	44	WN,b
1890	Kepler-1002	19323+4304	14.5643	144.3	0.4063	2.88	692	40	GD
1890	Kepler-1002	19323+4304	14.5643	144.3	0.4077	2.77	880	50	GD
1890	Kepler-1002	19323+4304	16.8631	143.7	0.4125	2.74	832	40	WN
1890	Kepler-1002	19323+4304	16.8631	144	0.4043	3.13	562	44	WN
1890	Kepler-1002	19323+4304	16.8768	143.5	0.4117	2.77	832	40	WN
1890	Kepler-1002	19323+4304	16.8768	143.7	0.4074	3.29	562	44	WN
1890	Kepler-1002	19323+4304	17.2555	144.2	0.4073	2.8	832	40	WN
1890	Kepler-1002	19323+4304	17.2555	143	0.4084	3.15	562	44	WN
1890	Kepler-1002	19323+4304	22.8753	142.8	0.4007	2.96	692	40	AD
1890	Kepler-1002	19323+4304	22.8753	144.1	0.3989	2.66	880	50	AD
1962		18569+4048	14.5612	113.9	0.1218	0.12	692	40	GD,b
1962		18569+4048	14.5612	114.2	0.1221	0.24	880	50	GD,b

Table 5. KOI Speckle Measurements

KOI no.	Exoplanet system	WDS	Date (2000+)	θ (°)	ρ (")	Δm (mag)	λ (nm)	$\Delta\lambda$ (nm)	Tel., Inst., and notes[c]
1962		18569+4048	16.8548	114.6	0.1268	0.2	832	40	WN
1962		18569+4048	16.8548	113.8	0.1278	0.13	562	44	WN
1962		18569+4048	17.2036	114	0.1279	0.16	832	40	WN
1962		18569+4048	17.2036	114.1	0.1293	0.23	562	44	WN
1962		18569+4048	22.7441	116.1	0.1284	0	692	40	AD,*b*
1962		18569+4048	22.7441	115.9	0.1325	0.02	880	50	AD,*b*
1989	Kepler-1040	18525+4808	15.5249	39.4	0.8078	3.99	692	40	GD
1989	Kepler-1040	18525+4808	15.5249	40.1	0.8136	4.17	880	50	GD
1989	Kepler-1040	18525+4808	15.5277	39.7	0.8091	6.09	692	40	GD
1989	Kepler-1040	18525+4808	15.5277	39.1	0.8052	5.1	880	50	GD
2059	Kepler-1076	19104+5104	14.5476	289.5	0.3869	1.14	692	40	GD
2059	Kepler-1076	19104+5104	14.5476	289.6	0.3872	0.84	880	50	GD
2059	Kepler-1076	19104+5104	14.5612	289.5	0.3864	0.96	692	40	GD
2059	Kepler-1076	19104+5104	14.5612	289.7	0.3868	0.78	880	50	GD
2059	Kepler-1076	19104+5104	16.8055	289.1	0.3947	1.58	832	40	WN
2059	Kepler-1076	19104+5104	16.8055	289.2	0.3889	1.42	562	44	WN
2059	Kepler-1076	19104+5104	17.2636	288.7	0.387	0.66	832	40	WN
2059	Kepler-1076	19104+5104	17.2636	289	0.3885	1.3	562	44	WN
2418	Kepler-1229	19499+4700	15.5335	344.3	0.1013	3.29	880	50	GD
2463	Kepler-1248	19122+5121	15.8199	127.3	0.6084	0.8	692	40	WD
2463	Kepler-1248	19122+5121	15.8199	127.4	0.6071	0.69	880	50	WD
2463	Kepler-1248	19122+5121	16.8056	308.3	0.6166	0.31	832	40	WN
2463	Kepler-1248	19122+5121	16.8056	306.5	0.608	0.7	562	44	WN
2754	Kepler-1339	18550+4822	12.7453	260.4	0.7785	<3.13	692	40	WD,*a*
2754	Kepler-1339	18550+4822	12.7453	260.6	0.7742	<2.39	880	50	WD,*a*
2754	Kepler-1339	18550+4822	13.7336	260	0.7803	<2.8	692	40	WD,*a*
2754	Kepler-1339	18550+4822	13.7336	260.4	0.7756	<2.53	880	50	WD,*a*
2754	Kepler-1339	18550+4822	14.5638	260.5	0.776	2.95	692	40	GD
2754	Kepler-1339	18550+4822	14.5638	260.7	0.7733	2.52	880	50	GD
2754	Kepler-1339	18550+4822	16.8029	260.7	0.7718	<2.47	832	40	WN,*a*
2754	Kepler-1339	18550+4822	17.2692	260.3	0.7769	2.54	832	40	WN
2754	Kepler-1339	18550+4822	17.2692	260.3	0.775	3.34	562	44	WN
2754	Kepler-1339	18550+4822	23.8009	263.6	0.8218	<2.7	880	50	AD,*a*
2837	Kepler-1364	19406+4935	13.406	138.3	0.35	0	692	40	WD
2837	Kepler-1364	19406+4935	13.406	137.4	0.3462	0	880	50	WD
2837	Kepler-1364	19406+4935	13.7285	136.7	0.3528	0.31	692	40	WD
2837	Kepler-1364	19406+4935	13.7285	137.5	0.3564	1.07	880	50	WD
2837	Kepler-1364	19406+4935	16.8712	135.9	0.3512	0.94	832	40	WN,*b*
2837	Kepler-1364	19406+4935	16.8712	136.2	0.3546	0.92	562	44	WN,*b*
2879		19468+4231	12.7511	110.4	0.4371	0.47	692	40	WD
2879		19468+4231	12.7511	109.5	0.434	0	880	50	WD
2879		19468+4231	16.8711	290.6	0.4421	0.41	832	40	WN
2879		19468+4231	16.8711	290.5	0.4407	0.77	562	44	WN
2904	Kepler-1382	19415+3903	12.7455	225.8	0.69	3.05	692	40	WD
2904	Kepler-1382	19415+3903	13.7283	226	0.7011	3.21	692	40	WD
2904	Kepler-1382	19415+3903	13.7283	225.5	0.6901	2.76	880	50	WD

Table 5. KOI Speckle Measurements

KOI no.	Exoplanet system	WDS	Date (2000+)	θ (°)	ρ (")	Δm (mag)	λ (nm)	$\Delta\lambda$ (nm)	Tel., Inst., and notes[c]
2904	Kepler-1382	19415+3903	13.7309	225.5	0.6905	3.2	692	40	WD
2904	Kepler-1382	19415+3903	13.7309	226	0.6919	2.85	880	50	WD
2904	Kepler-1382	19415+3903	14.5615	225.8	0.6927	3.23	692	40	GD
2904	Kepler-1382	19415+3903	14.5615	225.9	0.6922	3.09	880	50	GD
2904	Kepler-1382	19415+3903	16.8659	226.5	0.6927	2.95	832	40	WN
3020		19382+4411	13.4059	272.5	0.3758	2.54	692	40	WD
3020		19382+4411	13.4059	268.7	0.3697	2.11	880	50	WD
3020		19382+4411	13.7309	273.4	0.3814	2.13	692	40	WD
3020		19382+4411	13.7309	273.3	0.3867	2.01	880	50	WD
3020		19382+4411	17.2774	272	0.3734	2.18	832	40	WN
3020		19382+4411	17.2774	272.3	0.3726	2.94	562	44	WN
3156		19190+3916	15.7434	202.7	1.1363	<1.99	692	40	WD,a
3156		19190+3916	15.7434	202.7	1.1401	<1.59	880	50	WD,a
3156		19190+3916	16.8002	203.3	1.1308	<1.75	832	40	WN,a
3156		19190+3916	16.8741	203	1.1333	<2.3	832	40	WN,a
3156		19190+3916	16.8741	202.7	1.1321	<3.71	562	44	WN,a
3156		19190+3916	22.3616	202.8	1.1192	<2.13	692	40	AD,a
3156		19190+3916	22.3616	202.8	1.1174	<1.79	880	50	AD,a
3156		19190+3916	22.8672	202.8	1.1127	<2.1	692	40	AD,a
3156		19190+3916	22.8672	202.9	1.1137	<1.75	880	50	AD,a
3168		19093+3932	14.5641	332.1	0.8043	5.28	692	40	GD
3168		19093+3932	14.5641	332.4	0.8088	4.49	880	50	GD
3207		19130+4607	15.757	50.2	0.0723	0.69	692	40	WD
3207		19130+4607	15.757	231.3	0.0771	1.54	880	50	WD
3207		19130+4607	17.3892	234.1	0.0918	1.01	832	40	WN
3207		19130+4607	17.3892	231.8	0.0915	1.19	562	44	WN
3214AB		19547+4348	13.7282	319.2	0.4834	1.43	692	40	WD
3214AB		19547+4348	13.7282	317.2	0.4771	1.22	880	50	WD
3214AB		19547+4348	16.8712	318.4	0.4836	1.43	832	40	WN
3214AB		19547+4348	16.8712	318.2	0.4839	1.58	562	44	WN,b
3214AB		19547+4348	17.3893	318.4	0.491	<1.54	832	40	WN,a
3214AB		19547+4348	17.3893	318	0.4871	<1.42	562	44	WN,a
3214AB		19547+4348	22.7442	318.1	0.4869	1.4	692	40	AD
3214AB		19547+4348	22.7442	318.1	0.485	1.27	880	50	AD
3214AC		19547+4348	13.7282	200	1.3058	<3.08	880	50	WD,a
3214AC		19547+4348	16.8712	199.3	1.2966	<2.81	832	40	WN,a
3214AC		19547+4348	16.8712	201	1.3039	<2.99	562	44	WN,a
3214AC		19547+4348	17.3893	199.9	1.2879	<2.86	832	40	WN,a
3214AC		19547+4348	17.3893	200.2	1.2899	<3.09	562	44	WN,a
3214AC		19547+4348	22.7442	199.7	1.3043	<2.76	692	40	AD,a
3214AC		19547+4348	22.7442	199.5	1.3064	<2.51	880	50	AD,a
3234	Kepler-1443	18537+4704	14.5638	123.3	0.0646	0.75	692	40	GD
3234	Kepler-1443	18537+4704	14.5638	123	0.0644	0.69	880	50	GD
3234	Kepler-1443	18537+4704	17.3649	118.8	0.0867	0.91	832	40	WN
3234	Kepler-1443	18537+4704	17.3649	117.5	0.0743	0.4	562	44	WN
3471		19487+5009	14.5616	229.3	0.532	3.82	692	40	GD

Table 5. KOI Speckle Measurements

KOI no.	Exoplanet system	WDS	Date (2000+)	θ (°)	ρ (”)	Δm (mag)	λ (nm)	$\Delta\lambda$ (nm)	Tel., Inst., and notes[c]
3471		19487+5009	14.5616	228.9	0.5272	2.78	880	50	GD
3471		19487+5009	16.8658	229.1	0.5471	<2.81	832	40	WN,a
4203		19042+3859	13.4032	41.3	1.1502	<0.85	692	40	WD,a
4203		19042+3859	13.4032	41.3	1.1432	<0.84	880	50	WD,a
4203		19042+3859	16.8657	41.2	1.1524	<0.99	832	40	WN,a
4203		19042+3859	16.8657	41.1	1.1602	<1.04	562	44	WN,a
4273		19368+4629	14.7493	353.6	0.1786	2.03	692	40	LD
4273		19368+4629	14.7493	352.1	0.1758	1.89	880	50	LD
4273		19368+4629	17.3621	352.9	0.1748	1.77	832	40	WN
4273		19368+4629	17.3621	354.8	0.1775	1.74	562	44	WN
4287		19218+4840	13.4033	78.2	0.5788	1.58	692	40	WD
4287		19218+4840	13.4033	78.2	0.5753	1.53	880	50	WD
4287		19218+4840	16.863	78.6	0.5783	1.57	832	40	WN
4287		19218+4840	16.863	78.4	0.5791	<1.79	562	44	WN,a
4287		19218+4840	17.2118	78.5	0.5775	1.55	832	40	WN
4287		19218+4840	17.2118	78.6	0.5784	1.74	562	44	WN
4287		19218+4840	22.8672	79	0.5815	<1.72	692	40	AD,a
4287		19218+4840	22.8672	78.9	0.5866	<1.5	880	50	AD,a
4399		18485+4418	13.7254	341.5	0.0867	1.63	692	40	WD
4399		18485+4418	13.7254	167	0.0934	1.31	880	50	WD
5578		18573+4508	14.4625	98	0.3126	1.49	692	40	LD
5578		18573+4508	14.4625	97.7	0.3136	1.54	880	50	LD
5578		18573+4508	14.5612	97.9	0.3152	1.51	692	40	GD
5578		18573+4508	14.5612	98.3	0.3155	1.6	880	50	GD
5578		18573+4508	16.8547	97.7	0.3189	1.63	832	40	WN
5578		18573+4508	16.8547	97.7	0.321	1.54	562	44	WN
5578		18573+4508	17.3649	97.6	0.3206	1.57	832	40	WN
5578		18573+4508	17.3649	97.8	0.3197	1.52	562	44	WN
5578		18573+4508	22.8672	97.7	0.3314	1.56	692	40	AD
5578		18573+4508	22.8672	97.9	0.3327	1.57	880	50	AD
5822		19550+4757	14.7524	21.5	0.4237	0	692	40	LD,b
5822		19550+4757	14.7524	21.2	0.4253	0.05	880	50	LD,b
5822		19550+4757	16.7976	21.9	0.4169	0.36	832	40	WN
5822		19550+4757	16.7976	22.5	0.4086	0.4	562	44	WN
5822		19550+4757	17.3622	21.2	0.4216	0.25	832	40	WN
5822		19550+4757	17.3622	21.3	0.4226	0.35	562	44	WN
5822		19550+4757	22.8753	20.8	0.4272	0.18	692	40	AD,b
5822		19550+4757	22.8753	20.7	0.4282	0	880	50	AD,b
5822		19550+4757	23.801	20.6	0.4248	0.63	692	40	AD,b
5822		19550+4757	23.801	21.6	0.4278	0.24	880	50	AD,b
6109		19113+3913	14.7522	324	0.5231	2.6	692	40	LD
6109		19113+3913	14.7522	323.5	0.522	2.54	880	50	LD
6109		19113+3913	16.8001	143.6	0.5336	2.59	832	40	WN
6109		19113+3913	16.8001	322.8	0.5348	3.25	562	44	WN
7291		19556+4706	15.8116	80.4	0.1939	2.19	692	40	WD
7291		19556+4706	15.8116	80.9	0.1954	1.8	880	50	WD

Table 5. KOI Speckle Measurements

KOI no.	Exoplanet system	WDS	Date (2000+)	θ (°)	ρ (")	Δm (mag)	λ (nm)	$\Delta\lambda$ (nm)	Tel., Inst., and notes[c]
7291		19556+4706	16.8658	259	0.1895	1.91	832	40	WN
7291		19556+4706	16.8658	78.2	0.1806	1.84	562	44	WN
7291		19556+4706	16.8658	78.2	0.1806	1.84	562	44	WN

[a] The magnitude difference is reported for these targets as an upper limit due to the speckle decorrelation effect discussed in Horch et al. (2017).

[b] The position angle has been flipped 180 degrees to remain consistent with other measurements in either the table or other literature.

[c] The telescope and instrument used for each observation is abbreviated by: WN = WIYN 3.5 m and NESSI, WD = WIYN 3.5 m and DSSI, LD = LDT and DSSI, GD = Gemini-N 8.1 m and DSSI, and AD = ARC 3.5 m and DSSI.

B. PYTHON JUPYTER NOTEBOOK USED FOR CPM ANALYSIS

The following Python notebook was used to produce all updated $\Delta\mu_\alpha$, $\Delta\mu_\delta$, R_1, and R_2 values, updated dispositions, and plots presented in this thesis.

CPM Analysis

This notebook reads the data given in tables 1, 2, and 3 of Colton et al. (2021) remotely, as well as local .ptab files containing speckle data from APO. New speckle data is combined with the data given in Colton table 1 and used to calculate $\Delta\mu$, R_1 , and R_2 values. At the end of the notebook, dispositions of CPM, CPM?, LOS, or Uncertain are assigned to each system.

In 1

```
import urllib.request
import math
import numpy as np
import matplotlib.pyplot as plt
```

Executed at 2024.12.11 15:09:55 in 705ms

In 2

```
# Functions for calculating delta mu & errors

def sep_ra_trig(sep_list, pos_ang_list):
    sep_ra = []
    ind = 0
    for i in sep_list:
        pos_ang = pos_ang_list[ind]

        ra_comp = i * math.sin(math.radians(pos_ang))
        sep_ra.append(ra_comp)

        ind += 1
    return sep_ra


def sep_dec_trig(sep_list, pos_ang_list):
    sep_dec = []
    ind = 0
    for i in sep_list:
        pos_ang = pos_ang_list[ind]

        dec_comp = i * math.cos(math.radians(pos_ang))
        sep_dec.append(dec_comp)

        ind += 1
    return sep_dec


def calc_d_mu_ra(sep_list, pos_ang_list, epoch_list):
    sep_ra = sep_ra_trig(sep_list, pos_ang_list)
    slope, intercept = np.polyfit(epoch_list, sep_ra, 1)
    d_mu_ra = slope    # [arcsec/yr]
    d_mu_ra *= 1000    # [mas/yr]
    return d_mu_ra


def calc_d_mu_dec(sep_list, pos_ang_list, epoch_list):
    sep_dec = sep_dec_trig(sep_list, pos_ang_list)
    slope, intercept = np.polyfit(epoch_list, sep_dec, 1)
    d_mu_dec = slope    # [arcsec/yr]
    d_mu_dec *= 1000    # [mas/yr]
    return d_mu_dec
```

```python
def d_mu_ra_err(sep_list, pos_ang_list, epoch_list):
    sep_ra = sep_ra_trig(sep_list, pos_ang_list)
    coefficients, covariance_matrix = np.polyfit(epoch_list, sep_ra, 1, cov=True)
    slope_error = np.sqrt(covariance_matrix[0][0])
    slope_error *= 1000
    return slope_error


def d_mu_dec_err(sep_list, pos_ang_list, epoch_list):
    sep_dec = sep_dec_trig(sep_list, pos_ang_list)
    coefficients, covariance_matrix = np.polyfit(epoch_list, sep_dec, 1, cov=True)
    slope_error = np.sqrt(covariance_matrix[0][0])
    slope_error *= 1000
    return slope_error


def plot_d_mu_ra(koi_num, ymin=None, ymax=None, savefig=False, show_values=False, dr3_data=None):
    sep_list = sep_dict[koi_num]
    pos_ang_list = pos_ang_dict[koi_num]
    epoch_list = epoch_dict[koi_num]
    sep_ra = sep_ra_trig(sep_list, pos_ang_list)
    sep_range = max(sep_ra) - min(sep_ra)
    if show_values is True:
        print('Separations, range of RA separations, position angles, epochs, and sep_ra for KOI-'+koi_num)
        print(sep_list)
        print(sep_range)
        print(pos_ang_list)
        print(epoch_list)
        print(sep_ra)

```

```python
    x = np.array(epoch_list)
    y = np.array(sep_ra)
    slope, intercept = np.polyfit(x, y, deg=1)
    yfit = slope * x + intercept
    fig = plt.figure(figsize=(11,4))
    plt.scatter(x, y, s=9, color='black')
    plt.plot(x, yfit, lw=1.3, color='red')
    plt.xlabel('Besselian Epoch - 2000')
    plt.ylabel('Sep. in RA (arcsec)')
    plt.title('KOI-'+str(koi_num)+' (RA)')
    if ymin is not None and ymax is not None:
        plt.ylim(ymin, ymax)
    if dr3_data is not None:
        plt.scatter(16, dr3_data, s=40, marker='D', color='green')
    plt.show()
    if savefig is True:
        if dr3_data is not None:
            fig.savefig('koi'+str(koi_num)+'_ra_dr3.png', format='png')
        elif dr3_data is None:
            fig.savefig('koi'+str(koi_num)+'_ra.png', format='png')
    plt.close()


def plot_d_mu_dec(koi_num, ymin=None, ymax=None, savefig=False, show_values=False, dr3_data=None):
    sep_list = sep_dict[koi_num]
    pos_ang_list = pos_ang_dict[koi_num]
    epoch_list = epoch_dict[koi_num]
    sep_dec = sep_dec_trig(sep_list, pos_ang_list)
```

```python
    sep_range = max(sep_dec) - min(sep_dec)
    if show_values is True:
        print('Separations, range of Dec separations, position angles, epochs, and sep_dec for KOI-'+koi_num)
        print(sep_list)
        print(sep_range)
        print(pos_ang_list)
        print(epoch_list)
        print(sep_dec)

    x = np.array(epoch_list)
    y = np.array(sep_dec)
    slope, intercept = np.polyfit(x, y, deg=1)
    yfit = slope * x + intercept
    fig = plt.figure(figsize=(11,4))
    plt.scatter(x, y, s=9, color='black')
    plt.plot(x, yfit, lw=1.3, color='red')
    plt.xlabel('Besselian Epoch - 2000')
    plt.ylabel('Sep. in Dec (arcsec)')
    plt.title('KOI-'+str(koi_num)+' (Dec)')
    if ymin is not None and ymax is not None:
        plt.ylim(ymin, ymax)
    if dr3_data is not None:
        plt.scatter(16, dr3_data, s=40, marker='D', color='green')
    plt.show()
    if savefig is True:
        if dr3_data is not None:
            fig.savefig('koi'+str(koi_num)+'_dec_dr3.png', format='png')
        elif dr3_data is None:
            fig.savefig('koi'+str(koi_num)+'_dec.png', format='png')
    plt.close()
```

```python
def sep_ra_ranges():
    ra_range_dict = {}
    for koi, sep in sep_dict.items():
        sep_ra = sep_ra_trig(sep, pos_ang_dict[koi])
        sep_range = max(sep_ra) - min(sep_ra)
        ra_range_dict[koi] = sep_range
    return ra_range_dict


def sep_dec_ranges():
    dec_range_dict = {}
    for koi, sep in sep_dict.items():
        sep_dec = sep_dec_trig(sep, pos_ang_dict[koi])
        sep_range = max(sep_dec) - min(sep_dec)
        dec_range_dict[koi] = sep_range
    return dec_range_dict
```

Executed at 2024.12.11 15:09:55 in 7ms

Colton et al. Table 1

In 3

```python
# Table 1 -- speckle measurement data

table1 = 'https://content.cld.iop.org/journals/1538-3881/161/1/21/revision1/ajabc9aft1_mrt.txt'
file_object = urllib.request.urlopen(table1)
# lists of all koi numbers, dates, position angles, and separations -- honestly *probably unnecessary*
koi_nums = []
bess_dates = []
pos_angs = []
```

```python
seps = []
# dictionaries with koi numbers as keys, and lists of values corresponding to those koi nums
sep_dict = {}
pos_ang_dict = {}
epoch_dict = {}

row_ct = 1
for row in file_object:
    row = row.decode('utf-8')
    if row_ct > 37:                         # rows that contain data

        koi_num = row[:8].strip()
        koi_nums.append(koi_num)

        comp = row[5:8].strip()
        kep_num = row[8:20].strip()
        wds = row[20:31].strip()

        bess_date = float(row[31:39].strip())   # grabbing Besselian dates
        bess_dates.append(bess_date)            # adding them to list of all Besselian dates
        if koi_num not in epoch_dict.keys():    # appending dictionary with Besselian dates linked to observed KOIs
            epoch_dict[koi_num] = [bess_date]
        else:
            epoch_dict[koi_num].append(bess_date)

        pos_ang = float(row[39:45].strip())     # grabbing position angles
        pos_angs.append(pos_ang)                # adding them to list of all position angles
        if koi_num not in pos_ang_dict.keys(): # appending dictionary with position angles linked to observed KOIs
            pos_ang_dict[koi_num] = [pos_ang]
        else:
            pos_ang_dict[koi_num].append(pos_ang)

        sep = float(row[45:52].strip())         # grabbing separations
        seps.append(sep)                        # adding them to list of all separations
        if koi_num not in sep_dict.keys():      # appending dictionary with separations linked to observed KOIs
            sep_dict[koi_num] = [sep]
        else:
            sep_dict[koi_num].append(sep)

        lim_dmag = row[52:54].strip()
        dmag = float(row[54:59].strip())
        lam = int(row[59:63].strip())
        dlam = int(row[63:66].strip())          # FWHM of filter transmission
        notes = row[66:].strip()

        # print(koi_num, bess_date, pos_ang, sep)

    elif row_ct < 38:                       # rows that give info about the data
        print(row)

    row_ct += 1

file_object.close()
```

Executed at 2024.12.11 15:10:00 in 4s 515ms

```
> Title: Identifying Bound Stellar Companions to Kepler Exoplanet Host Stars Using\n\n       Speckle Imaging\n\nAuthors: …
```

Adding newer data

These functions are designed to read files of similar format to 'koi2223final.ptab' and append the new data to what's given in Colton et al. Table 1

Add Code Cell Add Markdown Cell

In 4

```
def strip_beginning_zeroes(string):       # helper function for reading target names out of APO .ptab files
    if string[-1:] == '0':
        string = string.strip('0')
        string = string+'0'
        return string
    else:
        return string.strip('0')


def add_new_data(filename, file_list):
    with open(filename, 'r') as file:
        lines = file.readlines()

    if filename not in file_list:
        file_list.append(filename)

        line_ct = 0
        for line in lines:
            if line_ct > 3:
                line = line.strip()
                koi_num = strip_beginning_zeroes(line[14:18])
                epoch = float(line[22:29])
                pos_ang = float(line[44:49].strip())
                sep = float(line[51:57])
                comp = line[77:79].strip()
                if comp == 'AB' or comp == 'AC':
                    koi_num += comp
                sep_dict[koi_num].append(sep)
                pos_ang_dict[koi_num].append(pos_ang)
                epoch_dict[koi_num].append(epoch)
            line_ct += 1
    else:
        return


seen_files = []     # this list stores names of data files that have already been added to avoid multiple copies of new data
```

Executed at 2024.12.11 15:10:00 in 3ms

In 5

```
add_new_data('koi2223final.ptab', seen_files)

# print(seen_files)
```

Executed at 2024.12.11 15:10:00 in 4ms

In 6

```
# making a list of all KOIs that have been observed

seen = set()
unique_kois = []
for item in koi_nums:
    if item not in seen:
        unique_kois.append(item)
        seen.add(item)

print("Number of unique KOI's:", len(unique_kois))
# print(unique_kois)
```

Executed at 2024.12.11 15:10:00 in 4ms

```
Number of unique KOI's: 60
```

In 7
```python
# counting number of independent epochs each KOI was observed

ind_epoch_dict = {}         # storing number of ind. epochs to their respective KOI number for ease of removal

for i in unique_kois:
    epoch_list = epoch_dict[i]
    seen = set()
    ind_epochs = []
    for x in epoch_list:
        if x not in seen:
            ind_epochs.append(x)
            seen.add(x)
    ind_epoch_dict[i] = len(ind_epochs)
```
Executed at 2024.12.11 15:10:00 in 11ms

As described in Colton et al. (2021), we do not run analysis on KOIs that have fewer than 3 independent observations

In 8
```python
removed_targets = []                  # a list of targets that were observed at fewer than 3 epochs
for koi, num in ind_epoch_dict.items():
    if num < 3:
        removed_targets.append(koi)
# print(removed_targets)

for target in removed_targets:          # removing the under-observed targets from dictionaries
    del sep_dict[target]
    del pos_ang_dict[target]
    del epoch_dict[target]

# print(sep_dict)
# print(pos_ang_dict)
```

Calculating average separation

The average separation of each system is used later in calculation of R2

In 9
```python
# this function takes in a dictionary of separations and outputs two dictionaries: one with average separations and one with corresponding errors, each still organized by KOI number

def run_ave_sep(sep_dict):
    ave_sep_dict = {}
    e_sep_dict = {}
    for koi, list in sep_dict.items():
        n = len(list)
        sum = 0
        for sep in list:
            sep *= 1000     # convert from arcsec to mas
            sum += sep
        ave = sum / n
        ave_sep_dict[koi] = ave

        sample_sum = 0
        for sep in list:
            sep *= 1000
            x = (sep - ave)**2
            sample_sum += x
        sample_sd = sample_sum / (n - 1)
        sample_sd **= 0.5
        e_sep_dict[koi] = sample_sd

    return ave_sep_dict, e_sep_dict
```
Executed at 2024.12.11 15:10:00 in 39ms

In 10

```
ave_sep_dict, e_sep_dict = run_ave_sep(sep_dict)
```

Executed at 2024.12.11 15:10:00 in 37ms

180° flips

In 11

```
### these targets had some angles flipped in the APO data — this is an ugly, but quick way of fixing that ###

# copy the SAs of target from pos_ang_dict into a list, then manually correct the angles which have been flipped 180°

# 1962 previously [113.9, 114.2, 114.6, 113.8, 114.0, 114.1, 296.1, 295.9]
angs_1962 = [113.9, 114.2, 114.6, 113.8, 114.0, 114.1, 116.1, 115.9]    # corrected

# 5822 previously [21.5, 21.2, 21.9, 22.5, 21.2, 21.3, 200.8, 200.7, 200.6, 201.6]
angs_5822 = [21.5, 21.2, 21.9, 22.5, 21.2, 21.3, 20.8, 20.7, 20.6, 21.6]    # corrected

pos_ang_dict['1962'] = angs_1962
pos_ang_dict['5822'] = angs_5822
```

Executed at 2024.12.11 15:10:00 in 47ms

Calculating $\Delta\mu$ values in RA and Dec for each KOI

This creates two dictionaries with KOI names as the keys and $\Delta\mu$ RA/Dec as the values, and two similar dictionaries to store uncertainties

In 12

```
d_mu_dec_dict = {}
e_dmd_dict = {}
d_mu_ra_dict = {}
e_dmr_dict = {}

for koi, list in sep_dict.items():
    s = list
    pa = pos_ang_dict[koi]
    e = epoch_dict[koi]
    d_mu_dec = calc_d_mu_dec(s, pa, e)
    d_mu_dec_dict[koi] = d_mu_dec
    e_dmd = d_mu_dec_err(s, pa, e)
    e_dmd_dict[koi] = e_dmd

for koi, list in sep_dict.items():
    s = list
    pa = pos_ang_dict[koi]
    e = epoch_dict[koi]
    d_mu_ra = calc_d_mu_ra(s, pa, e)
    d_mu_ra_dict[koi] = d_mu_ra
    e_dmr = d_mu_ra_err(s, pa, e)
    e_dmr_dict[koi] = e_dmr

# for key, value in d_mu_dec_dict.items():
#     print(value)
```

Executed at 2024.12.11 15:10:00 in 42ms

Plots

In 13

```
# I want the plots to have similar ranges in separation, so this cell finds the average separation range

ra_range_dict = sep_ra_ranges()
```

```
dec_range_dict = sep_dec_ranges()

strange_ra = {}
ave_ra_range = 0
n = 0
for koi, i in ra_range_dict.items():
    # print(koi, i)
    if i > 0.01 and i < 0.1:        # a few targets have unusual separation ranges, so not including those in average
        ave_ra_range += i
        n += 1
    else:
        strange_ra[koi] = i
ave_ra_range /= n

strange_dec = {}
ave_dec_range = 0
n = 0
for koi, i in dec_range_dict.items():
    print(koi, i)
    if i > 0.01 and i < 0.1:        # again, not including targets that have unusual separation ranges in average
        ave_dec_range += i
        n += 1
    else:
        strange_dec[koi] = i
ave_dec_range /= n

ra_graph_range = 1.5 * ave_ra_range     # using the average range in separation values to scale the range on plots
dec_graph_range = 1.5 * ave_dec_range

# print(ave_ra_range)
# print(ave_dec_range)
```
Executed at 2024.12.11 15:10:00 in 32ms

In 14

```
# This cell uses plot_d_mu_ra(KOI) and plot_d_mu_dec(KOI) to plot separation vs. time for the majority of systems

# These 13 targets have separation ranges which require different scalings; they are plotted separately
range_outliers = ['1','118','120','258AC','976','1119','1531','1792AB','1792AC','2754','2837','3020','3214AB']

for i in epoch_dict.keys():
    if i not in range_outliers:
        ave_sep = ave_sep_dict[i] / 1000
        pos_ang = pos_ang_dict[i][0]
        ave_sep_ra = ave_sep * math.sin(math.radians(pos_ang))
        ave_sep_dec = ave_sep * math.cos(math.radians(pos_ang))

        ra_min = ave_sep_ra - ra_graph_range
        ra_max = ave_sep_ra + ra_graph_range
        dec_min = ave_sep_dec - ra_graph_range
        dec_max = ave_sep_dec + ra_graph_range

        plot_d_mu_ra(i, ymin=ra_min, ymax=ra_max, savefig=False)          # plot sep in RA vs. time
        plot_d_mu_dec(i, ymin=dec_min, ymax=dec_max, savefig=False)       # plot sep in Dec vs. time
```
Executed at 2024.12.11 15:10:00 in 128ms

In 15

```
# This cell plots separation vs. time for the 13 systems with unusual average separations

savefig_param = False       # set to True when ready to save figures

for i in range_outliers:
    ave_sep = ave_sep_dict[i] / 1000
    pos_ang = pos_ang_dict[i][0]
    ave_sep_ra = ave_sep * math.sin(math.radians(pos_ang))
    ave_sep_dec = ave_sep * math.cos(math.radians(pos_ang))

```

```
    ra_min = ave_sep_ra - ra_graph_range
    ra_max = ave_sep_ra + ra_graph_range
    dec_min = ave_sep_dec - ra_graph_range
    dec_max = ave_sep_dec + ra_graph_range

    if i == '1':
        plot_d_mu_ra(i, ymin=ra_min+0.01, ymax=ra_max+0.01, savefig=savefig_param)
        plot_d_mu_dec(i, ymin=dec_min+0.01, ymax=dec_max+0.01, savefig=savefig_param)
    elif i == '258AC':
        plot_d_mu_ra(i, ymin=ra_min-0.04, ymax=ra_max+0.03, savefig=savefig_param)
        plot_d_mu_dec(i, ymin=dec_min-0.04, ymax=dec_max+0.03, savefig=savefig_param)
    elif i == '118':
        plot_d_mu_ra(i, ymin=-0.84, ymax=-0.71, savefig=savefig_param)
        plot_d_mu_dec(i, ymin=-1.35, ymax=-1, savefig=savefig_param)
    elif i in ['120','3214AB']:
        plot_d_mu_ra(i, ymin=ra_min-0.01, ymax=ra_max-0.01, savefig=savefig_param)
        plot_d_mu_dec(i, ymin=dec_min-0.01, ymax=dec_max-0.01, savefig=savefig_param)
    elif i in ['1119','3020']:
        plot_d_mu_ra(i, ymin=ra_min, ymax=ra_max, savefig=savefig_param)
        plot_d_mu_dec(i, ymin=dec_min-0.01, ymax=dec_max-0.01, savefig=savefig_param)
    elif i == '1531':
        plot_d_mu_ra(i, ymin=ra_min, ymax=ra_max, savefig=savefig_param)
        plot_d_mu_dec(i, ymin=dec_min+0.01, ymax=dec_max+0.01, savefig=savefig_param)
    elif i == '1792AB':
        plot_d_mu_ra(i, ymin=-0.75, ymax=-0.3, savefig=savefig_param)
        plot_d_mu_dec(i, ymin=-0.2, ymax=0.4, savefig=savefig_param)
    elif i == '1792AC':
        plot_d_mu_ra(i, ymin=1.5, ymax=1.9, savefig=savefig_param)
        plot_d_mu_dec(i, ymin=-1.1, ymax=-0.5, savefig=savefig_param)
    elif i == '2754':
        plot_d_mu_ra(i, ymin=ra_min-0.015, ymax=ra_max-0.015, savefig=savefig_param)
        plot_d_mu_dec(i, ymin=dec_min+0.015, ymax=dec_max+0.015, savefig=savefig_param)
    elif i in ['2837','976']:
        plot_d_mu_ra(i, ymin=ra_min+0.005, ymax=ra_max+0.005, savefig=savefig_param)
        plot_d_mu_dec(i, ymin=dec_min+0.005, ymax=dec_max+0.005, savefig=savefig_param)
```

Executed at 2024.12.11 15:10:00 in 124ms

Gaia DR3 data for resolved systems

In 16

```
gaia_ra_seps = {'13':-1.138534779,
                '118':-0.803869772,
                '120':1.207358008,
                '284':0.8592100315,
                '959':0.6112602753,
                '980':0.5061143584,
                '984':-1.168227852,
                '1792AC':1.725873555,
                '3156':-0.4440435574,
                '3214AC':-0.4353406849}

gaia_dec_seps = {'13':0.1992022409,
                 '118':-1.249821134,
                 '120':-0.997442991,
                 '284':-0.1143104746,
                 '959':-0.358071251,
                 '980':0.779049846,
                 '984':-1.30453446,
                 '1792AC':-0.7691206576,
                 '3156':-1.046964171,
                 '3214AC':-1.223403758}
```

Executed at 2024.12.11 15:10:00 in 132ms

In 17

```
# This cell plots separation vs. time for the systems which Gaia resolves including the data point from the previous cell

savefig_param = False

for i in gaia_ra_seps.keys():
    ave_sep = ave_sep_dict[i] / 1000
    pos_ang = pos_ang_dict[i][0]
    ave_sep_ra = ave_sep * math.sin(math.radians(pos_ang))
    ave_sep_dec = ave_sep * math.cos(math.radians(pos_ang))

    ra_min = ave_sep_ra - ra_graph_range
    ra_max = ave_sep_ra + ra_graph_range
    dec_min = ave_sep_dec - ra_graph_range
    dec_max = ave_sep_dec + ra_graph_range

    if i not in range_outliers:
        plot_d_mu_ra(i, ymin=ra_min, ymax=ra_max, savefig=savefig_param, dr3_data=gaia_ra_seps[i])
        plot_d_mu_dec(i, ymin=dec_min, ymax=dec_max, savefig=savefig_param, dr3_data=gaia_dec_seps[i])

    elif i in range_outliers:
        if i == '118':
            plot_d_mu_ra(i, ymin=-0.84, ymax=-0.71, savefig=savefig_param, dr3_data=gaia_ra_seps[i])
            plot_d_mu_dec(i, ymin=-1.35, ymax=-1, savefig=savefig_param, dr3_data=gaia_dec_seps[i])
        elif i == '120':
            plot_d_mu_ra(i, ymin=ra_min-0.01, ymax=ra_max-0.01, savefig=savefig_param, dr3_data=gaia_ra_seps[i])
            plot_d_mu_dec(i, ymin=dec_min-0.01, ymax=dec_max-0.01, savefig=savefig_param, dr3_data=gaia_dec_seps[i])
        elif i == '1792AC':
            plot_d_mu_ra(i, ymin=1.5, ymax=1.9, savefig=savefig_param, dr3_data=gaia_ra_seps[i])
            plot_d_mu_dec(i, ymin=-1.1, ymax=-0.5, savefig=savefig_param, dr3_data=gaia_dec_seps[i])

```

Executed at 2024.12.11 15:10:00 in 133ms

Calculating R1

First, we take the values for system PM used in Colton et al. (taken from Gaia DR2, Tycho-2, or UCAC4 proper motion catalogs)

Colton Table 2

In 20

```
table2 = 'https://content.cld.iop.org/journals/1538-3881/161/1/21/revision1/ajabc9aft2_mrt.txt'
file_object = urllib.request.urlopen(table2)

spec_pmRA_dict = {}
spec_pmRA_err_dict = {}
spec_pmDEC_dict = {}
spec_pmDEC_err_dict = {}

sys_pmRA_dict = {}
sys_pmRA_err_dict = {}
sys_pmDEC_dict = {}
sys_pmDEC_err_dict = {}

plx_dict = {}
e_plx_dict = {}

row_ct = 1
for row in file_object:
    if row_ct > 40:
        row = row.decode('utf-8')
```

```
            koi_num = row[:8].strip()
            comp = row[4:8].strip()
            kep_num = row[8:13].strip()
            f_kep = row[13:16].strip()

            spec_pmRA = row[16:24].strip()
            spec_pmRA_dict[koi_num] = float(spec_pmRA)
            e_spec_pmRA = row[24:30].strip()
            spec_pmRA_err_dict[koi_num] = float(e_spec_pmRA)
            spec_pmDEC = row[30:38].strip()
            spec_pmDEC_dict[koi_num] = float(spec_pmDEC)
            e_spec_pmDEC = row[38:44].strip()
            spec_pmDEC_err_dict[koi_num] = float(e_spec_pmDEC)

            sys_pmRA = row[44:53].strip()
            sys_pmRA_dict[koi_num] = float(sys_pmRA)     # appending dictionary with system PM (in RA) linked to observed KOIs
            e_sys_pmRA = row[53:59].strip()
            sys_pmRA_err_dict[koi_num] = float(e_sys_pmRA)
            sys_pmDEC = row[59:68].strip()
            sys_pmDEC_dict[koi_num] = float(sys_pmDEC)
            e_sys_pmDEC = row[68:74].strip()
            sys_pmDEC_err_dict[koi_num] = float(e_sys_pmDEC)

            prlx = row[74:80].strip()
            e_prlx = row[80:86].strip()
            if koi_num != '959':
                plx_dict[koi_num] = float(prlx)
                e_plx_dict[koi_num] = float(e_prlx)
            else:
                plx_dict[koi_num] = 28.041
                e_plx_dict[koi_num] = 0.462
            source = row[86:].strip()

            # print(row)
        elif row_ct < 41:
            print(row)
        row_ct += 1

file_object.close()
```

Executed at 2024.12.11 15:41:13 in 475ms

```
b'Title: Identifying Bound Stellar Comanions to Kepler Exoplanet Host Stars Using Speckle Imaging\n'\nb'Authors: Colton…
```

Combining system μ RA and Dec values into $|\mu_1|$ and storing in dictionaries

In [ ]:

```
def system_mu_math(mu_ra, mu_dec):
    mu1 = ((mu_ra)**2 + (mu_dec)**2) ** 0.5
    return mu1


def system_mu_err(mu_ra, mu_ra_err, mu_dec, mu_dec_err):
    mu1 = system_mu_math(mu_ra, mu_dec)
    nom = ((mu_ra * mu_ra_err)**2 + (mu_dec * mu_dec_err)**2) ** 0.5
    mu1_err = nom / mu1
    return mu1_err


def d_mu_math(d_mu_ra, d_mu_dec):
    d_mu = ((d_mu_ra)**2 + (d_mu_dec)**2) ** 0.5
```

```
    return d_mu


def d_mu_err(d_mu_ra, d_mu_ra_err, d_mu_dec, d_mu_dec_err):
    d_mu = d_mu_math(d_mu_ra, d_mu_dec)
    nom = ((d_mu_ra * d_mu_ra_err)**2 + (d_mu_dec * d_mu_dec_err)**2) ** 0.5
    d_mu_err = nom / d_mu
    return d_mu_err

#_______________________________________
sys_mu_dict = {}
e_sm_dict = {}

for koi, pmRA in sys_pmRA_dict.items():
    e_pmRA = sys_pmRA_err_dict[koi]
    pmDEC = sys_pmDEC_dict[koi]
    e_pmDEC = sys_pmDEC_err_dict[koi]
    # print(koi, pmRA, e_pmRA, pmDEC, e_pmDEC)

    sys_mu = system_mu_math(pmRA, pmDEC)
    e_sm = system_mu_err(pmRA, e_pmRA, pmDEC, e_pmDEC)
    sys_mu_dict[koi] = sys_mu
    e_sm_dict[koi] = e_sm

print(sys_mu_dict)

print(plx_dict)
```

In _
```
# updating system mu and plx values from Gaia DR3:

```

```
with open('updated_gaia_vars.txt', 'r') as file:
    for line in file:
        line = line.strip()
        # print(line)
        line = line.split('\t')
        if line[0] != 'KOI' and line[5] != '0':     # prevents from reading header line and any empty line
            koi_num = line[0]
            muRA = float(line[1])
            e_muRA = float(line[2])
            muDEC = float(line[3])
            e_muDEC = float(line[4])
            sys_mu = float(line[5])
            e_sys_mu = float(line[6])
            plx = float(line[7])
            e_plx = float(line[8])

            sys_mu_dict[koi_num] = sys_mu
            e_sm_dict[koi_num] = e_sys_mu
            plx_dict[koi_num] = plx
            e_plx_dict[koi_num] = e_plx
```

R1 functions

$$R_1 = \frac{|\Delta\mu|}{|\mu_1|}$$

In _
```
def run_r1(d_mu_ra_dict, d_mu_dec_dict, sys_mu_dict):
    r1_dict = {}
    for koi, sys_mu in sys_mu_dict.items():
```

```python
        d_mu_ra = d_mu_ra_dict[koi]
        d_mu_dec = d_mu_dec_dict[koi]
        r1 = ((d_mu_ra**2 + d_mu_dec**2)**0.5) / sys_mu
        r1_dict[koi] = r1
    return r1_dict


def run_r1_err(dmr_dict, e_dmr_dict, dmd_dict, e_dmd_dict, sm_dict, e_sm_dict):
    e_r1_dict = {}
    for koi, sys_mu in sm_dict.items():
        d_mu_ra = dmr_dict[koi]
        e_d_mu_ra = e_dmr_dict[koi]
        d_mu_dec = dmd_dict[koi]
        e_d_mu_dec = e_dmd_dict[koi]
        e_sys_mu = e_sm_dict[koi]

        r1 = ((d_mu_ra ** 2 + d_mu_dec ** 2) ** 0.5) / sys_mu
        l_nom = (d_mu_ra * e_d_mu_ra) ** 2 + (d_mu_dec * e_d_mu_dec) ** 2
        l_den = (d_mu_ra ** 2 + d_mu_dec ** 2) ** 2
        r = (e_sys_mu / sys_mu) ** 2

        e_r1 = r1 * ((l_nom / l_den + r) ** 0.5)
        e_r1_dict[koi] = e_r1

    return e_r1_dict
```

Executed at 2024.12.11 15:10:00 in 117ms

In _

```python
r1_dict = run_r1(d_mu_ra_dict, d_mu_dec_dict, sys_mu_dict)
e_r1_dict = run_r1_err(d_mu_ra_dict, e_dmr_dict, d_mu_dec_dict, e_dmd_dict, sys_mu_dict, e_sm_dict)

# "paper" referes to the Colton et al. (2021) paper, which is calculated here for comparison
paper_r1_dict = run_r1(spec_pmRA_dict, spec_pmDEC_dict, sys_mu_dict)
paper_e_r1_dict = run_r1_err(spec_pmRA_dict, spec_pmRA_err_dict, spec_pmDEC_dict, spec_pmDEC_err_dict, sys_mu_dict, e_sm_dict)
```

In _

```python
for koi, r1 in r1_dict.items():
    print(r1)
```

R2 functions

In _

```python
def r2_helper(d_mu, sep, plx, mass):
    r2 = (d_mu * (sep**0.5)) / (4.6 * ((plx**3)*mass)**0.5)
    return r2


def run_r2(d_mu_ra_dict, d_mu_dec_dict, sep_dict, plx_dict, mass_dict):
    r2_dict = {}
    for koi, mass in mass_dict.items():
        d_mu_ra = d_mu_ra_dict[koi]
        d_mu_dec = d_mu_dec_dict[koi]
        d_mu = d_mu_math(d_mu_ra, d_mu_dec)

        sep = sep_dict[koi]
        plx = plx_dict[koi]

        r2 = r2_helper(d_mu, sep, plx, mass)
        r2_dict[koi] = r2

    return r2_dict
```

```python


def e_r2_helper(d_mu, e_d_mu, sep, e_sep, plx, e_plx, mass, shoot=False):
    r2 = r2_helper(d_mu, sep, plx, mass)
    d_mu_term = (e_d_mu/d_mu)**2
    sep_term = (e_sep/(2*sep))**2
    plx_term = ((3*e_plx)/(2*plx))**2
    mass_term = 1/(200*(mass**2))
    e_r2 = r2 * ((d_mu_term + sep_term + plx_term + mass_term)**0.5)
    if shoot is True:
        return (e_r2, r2, d_mu, e_d_mu, sep, e_sep, plx, e_plx, mass, d_mu_term, sep_term, plx_term, mass_term)
    else:
        return e_r2

def run_r2_err(dmr_dict, e_dmr_dict, dmd_dict, e_dmd_dict, sep_dict, e_sep_dict, plx_dict, e_plx_dict, mass_dict, shoot=False):
    e_r2_dict = {}
    for koi, mass in mass_dict.items():
        d_mu_ra = dmr_dict[koi]
        d_mu_dec = dmd_dict[koi]
        d_mu = d_mu_math(d_mu_ra, d_mu_dec)
        e_d_mu_ra = e_dmr_dict[koi]
        e_d_mu_dec = e_dmd_dict[koi]
        e_d_mu = d_mu_err(d_mu_ra, e_d_mu_ra, d_mu_dec, e_d_mu_dec)
        sep = sep_dict[koi]
        e_sep = e_sep_dict[koi]
        plx = plx_dict[koi]
        e_plx = e_plx_dict[koi]

        if shoot is True:
            e_r2 = e_r2_helper(d_mu, e_d_mu, sep, e_sep, plx, e_plx, mass, shoot=True)
        else:
            e_r2 = e_r2_helper(d_mu, e_d_mu, sep, e_sep, plx, e_plx, mass)
        e_r2_dict[koi] = e_r2

    return e_r2_dict
```

Colton Table 3

Reading in the final determinations as well as the masses given in Colton et al. table 3

In [ ]:
```python
table3 = 'https://content.cld.iop.org/journals/1538-3881/161/1/21/revision1/ajabc9aft3_mrt.txt'
file_object = urllib.request.urlopen(table3)

mass_dict = {}

row_ct = 1
for row in file_object:
    row = row.decode('utf-8')
    if row_ct > 39:
        koi_num = row[:6].strip()
        m1 = row[37:42].strip()
        m2 = row[42:47].strip()
        m = float(m1) + float(m2)
        mass_dict[koi_num] = round(m, 2)
        r1 = row[49:56].strip()
        e_r1 = row[56:63].strip()
        r2 = row[63:70].strip()
        e_r2 = row[70:77].strip()
        notes = row[77:].strip()
```

```
        # print(round(float(m2), 2))
    else:
        # print(row)
    row_ct += 1

file_object.close()
```

Calculating R2

These are all of the variables needed to calculate R2 and respective errors

d_mu_ra_dict, e_dmr_dict, d_mu_dec_dict, e_dmd_dict, ave_sep_dict, e_sep_dict, plx_dict, e_plx_dict, mass_dict

In _
```
r2_dict = run_r2(d_mu_ra_dict, d_mu_dec_dict, ave_sep_dict, plx_dict, mass_dict)
e_r2_dict = run_r2_err(d_mu_ra_dict, e_dmr_dict, d_mu_dec_dict, e_dmd_dict, ave_sep_dict, e_sep_dict, plx_dict, e_plx_dict, mass_dict)
```

In _
```
for koi, r2 in r2_dict.items():
    print(r2)
```

Dispositions

Examining the relationships between R1 and its error, and R2 and its error, according to the guidelines given in Colton et al. to determine whether each target is CPM, CPM?, LOS, or Uncertain

In _
```
def give_disp_dict(r1_dict, e_r1_dict, r2_dict, e_r2_dict):
    disp_dict = {}

    for koi, r1 in r1_dict.items():
        e_r1 = e_r1_dict[koi]
        r2 = r2_dict[koi]
        e_r2 = e_r2_dict[koi]

        if r1 - e_r1 > 0.32 and r2 - e_r2 > 1.87:
            disp = 'LOS'
        elif r1 + e_r1 < 0.32 and r2 - e_r2 < 1.87:
            disp = 'CPM'
        elif r1 < 0.32 and r2 - e_r2 < 1.87:
            disp = 'CPM?'
        else:
            disp = 'Uncertain'

        disp_dict[koi] = disp

    return disp_dict
```

In _
```
disp_dict = give_disp_dict(r1_dict, e_r1_dict, r2_dict, e_r2_dict)

for koi, disp in disp_dict.items():
    print(disp)
```

Distances

In _
```
dist_dict = {}
e_dist_up_dict = {}
```

```
e_dist_low_dict = {}

# read in koi_dists.txt, copied from an Excel sheet with distances to each KOI

with open('koi_dists.txt','r') as dists:
    lines = dists.readlines()
    for line in lines:
        line = line.strip()
        line = line.split('\t')
        koi = line[0]
        d = float(line[1])
        dist_dict[koi] = d
        d_plus = float(line[2])
        d_minus = float(line[3])
        e_dist_up_dict[koi] = d_plus
        e_dist_low_dict[koi] = d_minus

# print(dist_dict)
```

Plotting R1 v. distance

```
In _
x = dist_dict.values()
y = r1_dict.values()

y_errors = []
for i in e_r1_dict.values():
    y_errors.append(i)

plt.errorbar(x, y, yerr=y_errors, fmt='o', color='black', markersize=3, elinewidth=0.8, capsize=2.5)
plt.axhline(y=0.32, ls='--', c='green', lw=2)
plt.axhline(y=1.06, ls='--', c='red', lw=2)
plt.xlabel('Distance [pc]')
plt.ylabel('$R_1 = |\Delta\mu|/|\mu_1|$')
plt.title('$R_1$ vs. Distance')
plt.ylim(-0.1,2)
# plt.savefig('r1_v_dist_cutoffs(2).png')
plt.show()
plt.close()
```

Plotting log(R2) v. distance

```
In _
x = dist_dict.values()
log_r2 = []
for i in r2_dict.values():
    log_i = np.log10(i)
    log_r2.append(log_i)

up_e_logr2 = []
low_e_logr2 = []
for koi, i in e_r2_dict.items():
    r2 = r2_dict[koi]
    logr2 = np.log10(r2)
    up = r2 + i
    log_up = np.log10(up)
    log_up -= logr2
    up_e_logr2.append(log_up)
```

```python
    low = r2 - i
    if low >= 0:
        log_low = np.log10(low)
        log_low = logr2 - log_low
        low_e_logr2.append(log_low)
    elif low < 0:
        log_low = np.log10(0.001)       # a cheap way of avoiding log errors with a few of the targets
        log_low = logr2 - log_low
        low_e_logr2.append(log_low)

cutoff = 0.26
plt.errorbar(x, log_r2, yerr=[low_e_logr2, up_e_logr2], fmt='o', markerfacecolor='black', markeredgecolor='black', markersize=3, ecolor='black', elinewidth=0.8, capsize=2.5)
plt.axhline(y=0.26, linestyle='--', color='green', linewidth='2')
plt.axhline(y=-0.04, linestyle='--', color='red', linewidth='2')
plt.ylim(-1,3)
plt.xlabel('Distance [pc]')
plt.ylabel('log($R_2$) = log(|$\Delta\mu$|/|$\Delta\mu$(orb,avg)|)')
plt.title('log($R_2$) vs. Distance')
# plt.savefig('logr2_v_dist_cutoffs.png')
plt.show()
plt.close()
```